THE FLEXURAL RESPONSE OF CONCRETE BEAMS RETROFITTED WITH FRP AND FIBROUS CEMENTITIOUS COMPOSITES

A COMPARATIVE EXPERIMENTAL AND ANALYTICAL INVESTIGATION

A Thesis

Presented to

The Faculty of Engineering

At Notre Dame University - Louaize

In Partial Fulfillment

of the Requirements for the Degree of

Masters of Science in Civil Engineering

By

Christ Elie El Achkar

May 2023

Notre Dame University – Louaize
Faculty of Engineering

Department of Civil and Environmental Engineering

We hereby approve the thesis of

Christ Elie El Achkar,

Candidate for the Masters of Science in Civil Engineering

Signature

Dr. Sary Malak — Thesis Advisor

Signature

Dr. Talal Salem — Thesis Reader

DEDICATED TO

“My family, friends, and loved ones. A special feeling of gratitude to my parents for believing in me and providing me with the resources to pursue my dreams. I also owe a debt of gratitude to my thesis advisor, Dr. Sary A. Malak, whose guidance, expertise, and patience have been indispensable to the completion of this project.”

ACKNOWLEDGEMENTS

I would like to give my warmest thanks and deepest appreciation to my thesis supervisor Dr. Sary A. Malak who made this work possible. He continually conveyed a spirit of adventure for research, which was a major motivation for me. Dr. Malak helped me develop research skills throughout this project, for he directed me to the right path when it grew complicated.

I also would like to thank my thesis reader, Dr. Talal Salem, for his significant comments and suggestions that influenced my thesis's progression.

Further thanks to the NDU family for providing all the necessary equipment and tools for experimental testing and theoretical modeling.

ABSTRACT

The main objective of this study is to compare the flexural behavior of beams retrofitted at the tension face with Fiber Reinforced Polymers (FRP) such as Glass Fiber Reinforced Polymer (GFRP), Carbon Fiber Reinforced Polymer (CFRP), with cementitious fibrous composites such as Fiber Reinforced Concrete (FRC) and Slurry Infiltrated Fiber Reinforced Concrete (SIFCON). The tests were conducted on cast-in-place concrete beams in a single-point load bending application. Two batches of beams were considered unreinforced and reinforced with steel reinforcement at the tension face. The study aimed to examine their flexural behavior after retrofitting with the composite materials identified above. Theoretical models will be developed to compute the theoretical loads and deflections of beams retrofitted with GFRP, CFRP, FRC, and SIFCON to validate the experimental load-deflection curves. Mechanical parameters were obtained experimentally including ultimate load, ultimate deflection, rupture load, rupture deflection, stiffness, and toughness. This thesis aims to develop frameworks and guidelines for designing unreinforced and reinforced concrete beams retrofitted with different composite materials including cementitious fibrous and reinforced fiber polymers and to compare the results for constructability and application issues. The results of SIFCON Parallel and SIFCON Perpendicular extremely differ, having the only difference between the two composites being the fiber's orientation. This simple direction transforms the composite from the best to the worst composite between all other retrofits. Polymers are mainly recommended to handle gravity loads and SIFCON Parallel is suitable for earthquake and high impulse loadings. From the study above, it was noted that the performance of SIFCON parallel with steel reinforcement had a higher ultimate load capacity than without steel of around 22.54%. SIFCON parallel

reached the highest load capacity of 58.416 kN among all steel-reinforced specimens. SIFCON perpendicular and FRC resulted in the lowest and similar ultimate load capacity in the range of 29 kN, excluding regular concrete. From the comparison of polymers and cementitious composites without steel reinforcement, polymers primarily control the highest loads ranging from 40 to 50 kN as well as SIFCON parallel with 47.67 kN. It was discovered, however, that cementitious composites can maintain a significant amount of strength beyond peak levels in contrast to polymers, which tend to have a rapid failure right after peak loads. The rupture strains of SIFCON with fibers parallel to the load direction reached values of 8.1 mm compared to FRP reaching values of 4.4 mm.

Keywords: flexural behavior; fiber polymers; cementitious; mechanical parameters; composite materials

Table of Contents

List of Tables

List of Figures

1. INTRODUCTION

The use of Fiber Reinforced Polymers (FRP) has been extensively used in the industry to reinforce existing concrete beams for flexural resistance. The guide for the design and construction of externally bonded FRP systems for strengthening concrete (ACI 440.2R-17) has been adopted as the standard design code for FRP retrofits. Limited research has been developed with regards to retrofits of beams using cementitious composites including Fiber Reinforced Composites (FRC) and High-Performance Fiber Reinforced Cement Composites (HPFRCC); HPFRCC includes Slurry Infiltrated Fiber Concrete (SIFCON). The objective of this research is to compare the flexural behavior of beams retrofitted at the tension surface with GFRP, CFRP to FRC, and SIFCON.

Fiber Reinforced Polymers (FRP) are formed of carbon fibers in the form of two-dimensional grids of aligned fibers coated in a hardened resin with fillers and additives. During the 1990s, FRP reinforcements grabbed the attention of many researchers, who presented design guidelines for FRP Reinforced Concrete. The use of FRP as a structural reinforcement component has been extensively used in the industry and design guidelines have been globally published. Carbon fiber has many advantages including low density, low conductivity, high fatigue strength, high elastic modulus, good creep level, chemical effect resistance, and water resistance (FYFE). Nevertheless, it has low compressive strength and requires a relatively high-energy requirement for its production which leads to an increased cost.

The main advantages of GFRP are high strength, chemical effect resistance, water-resistant, and low cost. The low cost of GFRP compared to other forms of FRP encourages its widespread use in the construction industry. However, the main

disadvantages of GFRP include a relatively low elastic modulus, low resistance to alkalinity, and low long-term strength due to stress rupture.

Fiber Reinforced Concrete (FRC) is regular concrete strengthened with short, randomly oriented steel fibers. Only hooked-ended Steel fibers 50mm long with a diameter of 1mm were employed in the combination of FRC in the proposed study. Steel fibers are primarily used to offer post-cracking tension resistance to concrete elements (T.Y. Lim et al. 1987). FRC was not recognized as a structural material in the ACI Code 544.1 until 2008 when it was approved for the first time using deformed steel fibers as minimum shear reinforcement in beams.

Fiber Reinforced Concrete (FRC) and Slurry Infiltrated Fiber Concrete (SIFCON) are both relatively common. SIFCON differs from FRC in the following aspects: it contains sand and cement such as silica sand and micro silica and it has a significantly higher volume proportion of fibers, the fibers are perfectly aligned leading to better tensile performance. Additionally, the term slurry consists of a cement-based mix that possesses the physical characteristics of a flowable cement paste. This effect is due to the presence of fine particles mixed with cement and a superplasticizer. Fibers are pre-laid and then intermixed with slurry, allowing for a higher percentage of fiber volume fractions of 12%; while FRC fiber content can only go up to 2% volume fraction due to fiber balling during mixing. The compressive strength of the slurry is highly influenced by the water-cement ratio and fineness of the cement and sand. The alignment and volume fraction of the fibers are the most significant parameters that affect the tensile strength of SIFCON. SIFCON has aligned fibers and provides continuity which allows for a multiple cracking mechanism compared to a single crack mechanism as in FRC.

The goal of this work is to develop an experimental investigation of reinforced concrete beams retrofitted with fibrous cementitious composites and develop analytical models similar to those of FRP in the ACI code that will confirm the experimental results. Results will be compared to typical FRP retrofits summarizing conclusions and recommendations for beam retrofits.

2. PROBLEM STATEMENT

Typical reinforced concrete structures are vulnerable to extreme loading conditions requiring retrofits with high-tensile composite material. Retrofitting concrete structures with FRP has been widely used due to its high tensile strength and ease of applicability in the industry. However, it has several limitations and is not applicable in all possible cases, knowing that it has a brittle failure and does not exhibit a post-hardening behavior as cementitious composites. It also requires high-end substrate preparation through cleaning and sealing, providing surface flatness, and detailing corners. It is vulnerable when exposed to fire and is brittle in nature.

Hence, investigating the use of high energy absorption cementitious composite materials is warranted such as FRC and SIFCON for retrofitting purposes.

Several research questions arise, whether cementitious composites can be used in lieu of polymers to retrofit reinforced concrete beams. The proposed study herein will investigate which of the composites used for retrofitting can resist gravity loads (large peak loads) or which perform better under seismic or high impulse loading such as blast or impact (higher ductility).

3. RESEARCH OBJECTIVES

- Develop experimental data for the flexural response of beams retrofitted with FRP or cementitious composites.
- Develop analytical models used for the design of reinforced concrete reinforced with cementitious composites for future guidelines to be implemented and incorporated in ACI Codes, similar to FRP.
- Compare and summarize results between cementitious and FRP retrofits.

4. PROPOSED RESEARCH METHODOLOGY

The proposed research methodology includes a literature review to present available studies that were focused on retrofit options. Secondly, the experimental investigation includes the preparation of the concrete wood forms, mixing, pouring, curing of concrete, and integration of the composite material. Experimental testing of the retrofitted beams shall follow using Linear variable Direct Transducers (LVDTs) calibrated and installed to measure deflections. Data is extracted and experimental graphs will be plotted for further analysis. Analytical models will be developed to obtain the moment-curvature and load-deflection diagrams for each retrofit option. Theoretical graphs will be plotted to confirm the experimental results. All results will be compared and discussed to develop the most suitable retrofit technique based on the loading type requirement.

5. LITERATURE REVIEW

Many studies concentrated on the investigation of the flexural performance of concrete beams retrofitted with FRP composite materials. Limited research was conducted on the use of cementitious materials for retrofits such as FRC and SIFCON. However, many studies focused on constructing beams with FRC and SIFCON whereby the performance is not similar to retrofitting at tension face with such composite.

5.1 FRP RETROFIT

5.1.1 EXPERIMENTAL FRP LITERATURE REVIEW

ACI 440.2R-17 "Guide for the Design and Construction of Externally Bonded FRP Systems for Strengthening Concrete" states that FRP reinforcement placed at the tension face of a concrete flexural member with fibers along the length of the member will offer an increase in flexural strength. Meier and Kaiser 1991; Ritchie et al. 1991; Sharif et al. 1994 state that a 10 to 160 percent overall increase in flexural strength arises after the FRP is introduced into the system.

Bencardino, Condello, and Ombres (2016) executed a mathematical estimation and an infinite element investigation for 17 samples consisting of beams reinforced with FRP and steel bars. After comparing the arithmetical estimation and analytical results with the experimental results, they verified that the Finite Element (FE) model complied with a combination of international standards, such as ACI 440.1R-06 and fib Model Code 2010. The available data was limited to the experimental studies on FRP and

other types of reinforcing bars including theoretical equations. Hence, not enough data has been provided for the application in domestic conditions. The flexural behavior due to hybrid reinforcement was assessed and the reliability of the analysis model was examined. The results will be used as fundamental data for further relevant criteria.

GangaRao and Vijay (1998) examined the flexural failure modes for an FRP-strengthened member and the following was concluded:

a) Crushing of the concrete in compression before yielding the reinforcing steel

b) Yielding of the steel in tension followed by rupture of the FRP laminate

c) Yielding of the steel in tension followed by concrete crushing

d) Delamination of shear and tension of the concrete cover resulted

e) Debonding of FRP from the concrete substrate (FRP debonding)

H. Falah Hassan et al. (2020) studied the flexural performance of concrete beams reinforced by GFRP bars and strengthened by CFRP sheets. The beams have a length of 190 cm, width of 15 cm, and height of 20 cm; while the sheets have a 60 cm length and 15 cm wide that are placed at mid-span. The presented study consisted of significant experimental analysis of the flexural efficiency of reinforced concrete beams with GFRP bars and fortified by CFRP sheets. Ten GFRP-reinforced concrete beams were exposed to frequent loading series using a four-point bending system for the analysis. As the reinforcement ratio and the number of CFRP layers were increased, the crack sizes and central deflection were noticeably decreased. The failure in (GFRP RC) beams reinforced with more than the balanced reinforcement appears to fail in compression which resulted in concrete crushing. As the CFRP layers were increased from (0 layer, 1 layer, and 2 layers), this led to the increase of the ultimate capacity by

(68.75, 27, and 12.8) %, respectively. Six beams over-reinforced with GFRP bars failed by concrete crushing, whereas the under-reinforced beam failed by the rupture of GFRP bars. However, the under-reinforced beam reinforced with a twin CFRP sheet layer failed through the crushing of concrete.

Kinga Brózda et al. (2017) executed the flexural analysis of beams reinforced with FRP bars. CFRP reinforcement obtained the highest flexural strength of 22.14 kN.m in the computational analysis of beams reinforced with FRP bars. CFRP reinforcement resulted in about 30% higher than the flexural strength obtained by beam a reinforced with Aramid Fiber Reinforced Polymers (AFRP) bars. Beams retrofitted with GFRP bars resulted in the lowest nominal moment capacities. In addition, the smallest deflection value of 5.34 mm was reached in beams reinforced with AFRP bars.

Liu, Sun, and Wu (2019) observed the flexural capacity and deflection of fiber-reinforced lightweight aggregate concrete (LWC) beams reinforced with GFRP bars. Six LWC beams strengthened with glass fiber reinforced polymer (GFRP) and tested in four-point bending with and without steel fibers. The findings indicated that adding steel fibers and raising the reinforcing ratio reduced the strain on the FRP bars. The proposed model produced precise predictions for the ultimate moment, whereas the design codes underestimated the flexural capacity of the LWC beams with and without steel fibers. Additionally, the suggested short-term stiffness model yielded reasonable estimations of deflection for steel fiber-reinforced lightweight aggregate concrete (SFLWC) and fiber-reinforced normal weight concrete (FNWC) beams.

Qureshi and Saleem (2018) examined the flexural and shear strain characteristics of

carbon fiber-reinforced polymer composite adhered to a concrete surface. CFRP was used as an externally mounted flexural and shear reinforcement to strengthen the beams. Flexural load tests were executed on eight reinforced concrete beams. The cross-sectional measurements of each reinforced concrete beam chosen for testing were the same (100 mm × 200 mm), and they all had the same overall length of 1200 mm. The strain gauges were applied on the surface of concrete and CFRP strips to assess the strain of both CFRP and concrete under flexural and shear stresses. The resulting test data was presented in the form of load–deformation and strain values. The test results showed that the strength increment in flexural members is highly dependent on the strain values of the CFRP. The research indicates that increasing the external CFRP shear reinforcement in beams with a weak flexural behavior is not recommended to strengthen beams.

Yang et al. (2011) inspected the behaviors of beams reinforced with different types of bars and researched to find explanations for various problems such as premature debonding, cracking, and brittle failure of FRP-reinforced beams. To investigate the causes of the various issues seen in FRP-reinforced beams, ten experiments were conducted and analyzed. According to the study results, flexural strength and ductility of the retrofitted beams were significantly higher than those of the unretrofitted beams. However, the retrofitted beams exhibited premature debonding and reduced stiffness due to the low bond strength between the FRP sheets and concrete. The study highlights the importance of selecting the appropriate type of reinforcement and retrofitting material for concrete beams based on their specific requirements and structural behavior.

Bakhshi et al. (2019), a more recent study, looked into the flexural behavior of reinforced concrete beams that had been retrofitted with CFRP sheets. According to the findings, CFRP sheets significantly reduced crack width and deflection while also enhancing the flexural strength and ductility of the beams.

5.1.2 THEORETICAL FRP LITERATURE REVIEW

ACI 440 provides specifications for the design and construction of concrete structures strengthened with fiber-reinforced polymer (FRP) materials. In addition to practical recommendations, ACI 440 also includes mathematical models and equations for forecasting the behavior of FRP-strengthened concrete structures. The following equations are some of the most commonly used from ACI 440:

- Strain compatibility equation:

  Equations (5.1) and (5.2) are used to calculate the strain in the FRP reinforcement (ε_f) and the concrete substrate (ε_c) based on their respective moduli of elasticity (E_f, E_c) and the applied loads (P). Equation (5.2) for the strain in the substrate is obtained from Equation (5.1):

$$\varepsilon_f = \varepsilon_c \times \left(\frac{E_c}{E_f}\right) + \left(P \times \frac{L}{A_f} \times E_f\right) \qquad Eq\ (5.1)$$

$$\varepsilon_c = \varepsilon_f \times \left(\frac{E_f}{E_c}\right) - \left(P \times \frac{L}{A_c} \times E_c\right) \qquad Eq\ (5.2)$$

  where L is the length of the beam, A_f and A_c are the areas of the FRP and concrete, respectively.

- FRP tensile strength equation:

  Equation (5.3) is used to calculate the tensile strength of the FRP reinforcement (f_f) that is founded on the ultimate tensile strength of the fiber (f_t) and the safety factor (φ):

$$f_f = \varphi \times f_t \qquad Eq\ (5.3)$$

  Where the value of φ is deteremined by the level of confidence and reliability needed for the particular application, as well as the statistical distribution of the important safety elements. The ACI 440 standard recommends values of φ for various FRP materials and applications.

- FRP strain limit equation:

  The following equation (5.4) is used to calculate the allowable tensile strain in the FRP reinforcement ($\varepsilon_{f,max}$) based on the ultimate tensile strain of the fiber (ε_t) and the safety factor (φ), which is the same factor as for equation (5.3):

$$\varepsilon_{f,max} = \varphi \times \varepsilon_t \qquad (Eq.5.4)$$

J.G. Teng et al. (2006) studied the debonding failure of FRP-to-concrete interfaces by developing a theoretical model. The performance of the interface between FRP and concrete is a major factor that affects the behavior of the retrofitted structure. Two types of debonding failures have been commonly observed: plate-end debonding and intermediate crack-induced debonding. This paper presents an analytical model for the debonding process in an FRP-to-concrete bonded joint model where the FRP plate is subject to tension at both ends. A realistic bi-linear local bond-slip law is employed.

Expressions for the interfacial shear stress distribution and the load-displacement response are derived for different loading stages. Results from the analytical solution are presented to demonstrate how the bond length affects the behavior of such bonded joints. While the emphasis of the paper is on FRP-to-concrete joints, the analytical solution is valid for similar joints between thin plates of other materials (e.g. steel and aluminum) and concrete. The theoretical solution has determined five possible failures for FRP-to-concrete interfaces that are a plate-end debonding failure, intermediate crack-induced debonding failure, debonding failure due to excessive interfacial shear stress, debonding failure due to excessive interfacial normal stress, combination of intermediate crack-induced, and shear stress-induced debonding failure.

The delamination strain is a crucial factor in defining the bond-slip behavior between the FRP plate and the concrete substrate. The delamination strain can be determined using the formula shown below, per ACI 440.2R-08:

$$e_{fd} = 0.41\sqrt{\frac{f_c^{'}}{t_f\, m\, E_f}} \leq 0.9e_{fu} \quad \text{in SI units} \qquad (Eq.\,5.5)$$

Where e_{fd} is the delamination strain, e_{fu} represents the ultimate strain, t_f is the thickness of the polymer, m is the number of polymer sheet layers, and E_f is the modulus of elasticity of the polymer. To avoid such an intermediate crack-induced debonding failure mode, the effective strain in FRP reinforcement must be restricted to the strain level at which debonding may occur, as defined in Eq. 5.5. The delamination equation can be used to design composite structures that are more resistant to failure by foreseeing how composite materials would respond to flexural loads. By determining the effective flexural stiffness of a composite beam, engineers may

forecast the deflection and stress distribution in the beam under different loading conditions.

Moon, Oh, and Ahn (2008) developed a finite element model to analyze the flexural behavior effect of FRP-reinforced beam design variables. The model was verified by relating its results to the experimental results. The manipulated variables were the reinforcement ratio, elasticity modulus of FRP, and compressive strength of concrete. The effect of the variables on the flexural rigidity of the members and the deflection displacement were compared to the theoretical values in ACI 440. The investigation showed that the behavior was mostly influenced by the reinforcement ratio and the increase in the compressive strength of concrete.

Wang and Chen (2003) worked on an analytical study on reinforced concrete beams strengthened for flexure and shear with composite plates. The study involved a test for 5 m long retrofitted T-beams simply supported on four points tested under monotonic load to verify the analytical model.

The internal moment of resistance as shown in eqution (5.6) is then obtained by taking the moments of internal forces about the neutral axis.

$$M = C_c\bar{y}_c + \sum_{i=1}^{n} f_{si}A_{si}(d_i - c) + f_pA_p\left(d_p - c\right) \qquad Eq.(5.6)$$

Where C_c is the sectional compressive force due to compressive stresses in the concrete, $\bar{y}_c$ is the distance of the resultant force measured from the neutral axis, f_{si} is the steel yield strength, A_{si} is the area of steel reinforcement, d_i is a distance

measured from the top concrete fiber to the centroid of steel bar in a layer i, c is the depth measured from the sectional extreme compression resultant force to the neutral axis, f_p is the tensile stress in the FRP plate, A_p is the cross-section area of FRP plates, and d_p is a distance measured from the top concrete fiber to the centroid of FRP plate.

The curvature by definition is as in equation (5.7):

$$\phi = \frac{\varepsilon_{ct}}{c} \qquad Eq.(5.7)$$

Where ϕ is the beam curvature and ε_{ct} is the concrete strain in the extreme fiber of the cross section.

The major assumptions used in the theoretical model were considering the plane sections remain plane when subjected to bending, perfect bond exists between the composite plate and concrete beam, and the bonding agent layer between the composite plate and the reinforced concrete beam is disregarded. The predicted model builds upon discrete element analytical methodology incorporating the dual effects of flexure and shear in beams. An important conclusion in this paper is that the predicted model can be used to accurately predict the behavior of load versus displacement and FRP plate bond stresses. Test results verified the model assumption of strain compatibility and that no bond slip between the concrete surface and FRP plate is satisfactory.

5.2 FRC RETROFIT

Very limited information has been provided in relation to any theoretical modeling of concrete beams retrofitted with FRC as well as for reinforced beams rotriftted with FRC.

5.2.1 EXPERIMENTAL FRC RETROFIT LITERATURE REVIEW

Bhawuk Verma (2015) studied the use of steel fiber-reinforced concrete (SFRC) over plain concrete for shotcrete by comparing their compressive and flexural strengths. The flexural strength testing was performed using a normal concrete beam of size 700 mm x150 mm x150 mm by a two point loading method. The results showed that SFRC has a higher flexural strength than plain concrete, with larger aspect ratios leading to greater flexural strength when compared to plain concrete. Hence, the introduction of steel fibers to the concrete sample increased its load capacity.

Fatih Altun et al. (2006) studied the effects of steel fiber addition on the mechanical properties of concrete and reinforced concrete beams. It was concluded that the reinforced-concrete beams having a 30 kg/m^3dosage of steel fibers resulted in an noticeable increase in the ultimate loads and flexural toughness relative to those reinforced concrete beams without steel fibers.

Mohd Muzammil Ahmed and Mohd Majiduddin (2015) examined the flexural behavior of ternary blended steel fiber reinforced concrete beams using crimped fibers. The experiment tested beams of size 1400 mm ×100 mm ×150 mm subjected to two-point

loads at the age of 7 days and 28 days. This study showed that the flexural behavior of beams improved after including fibers. The flexural strength of the beam improved approximately by 21.58%. The increased moment capacity of beams having 0.5% of the fiber is 7.16%, for 0.75% of fibers the increase was 12.60%, while for 1.25% there was a 6.65% reduction. The moment carrying capacity of the beam increased by 21.58% after adding 1% crimped steel fiber. Greater elastic properties of specimens resulted after adding the percentage of fibers.

Raghunath and K.suguna (2015) have worked on the flexural behavior of high-strength steel fiber-reinforced concrete beams. A total of 4 beams of 3 m in length and 150 mm × 250 mm in cross-section were cast and tested. The different steel fibers volume were taken to be 0.5%, 1%, and 1.5%. Tests were conducted under a two-point load application. The beam specimen composed of a 1% fiber volume fraction of steel fiber resulted in the highest strength with a 30.03% increase and an enhanced ductility that increased around 41.34%. This suggests that the 1% fiber volume fraction was successful in increasing the strength and ductility of the beam while preserving an even distribution of fibers throughout the concrete matrix. Beyond this point, however, might have resulted in fiber clustering and the formation of voids, which would have decreased the beam's capacity.

Soulioti et al. (2009) have worked on the effects of fiber geometry and volume fraction on the flexural behavior of steel-fiber reinforced concrete beams. An investigation through this research focused on the compressive strength and flexural strength. The results were compared with unreinforced concrete. The test results showed that the fibers highly affect both the fresh state of the concrete and the mechanical properties

of hardened concrete samples. The comparison of load-displacement curves between normal concrete samples and samples intermixed with fibers showed that the change of fiber volume from 0%, 0.5%, 1%, and 1.5% resulted in an increase in the ultimate strength capacity of the specimens, respectively.

5.3 SIFCON RETROFIT

Very limited information has been provided in relation to any theoretical modeling of concrete beams retrofitted with SIFCON as well as for reinforced beams retrofitted with SIFCON. Limited research has been done to provide an overview of the use of SIFCON for retrofitting concrete beams.

5.3.1 EXPERIMENTAL SIFCON RETROFIT LITERATURE REVIEW

Mustaqqim et al. (2013) studied the flexural behavior of high-performance slurry-infiltrated fiber-reinforced concrete beams with different curing methods. The tests by two-point load application until failure recorded the prisms' behavior and the load-deflection response. After examining the outcomes of the experimental works, they concluded that the amount of steel fiber affects the strength of the beams. The flexural strength is increased constantly with an increment of steel fiber content. The highest content of hooked-end steel fiber of 5% volume fraction with an aspect ratio of 80 resulted in the highest strength.

An experimental investigation was carried out by Azhari et al. (2008) to assess the effectiveness of SIFCON for retrofitting reinforced concrete beams with insufficient

flexural capacity. Six reinforced concrete beam specimens measuring 150 mm × 250 mm × 2500 mm were used by the authors. In order to simulate the conditions of insufficient flexural capacity, the beams were built to have a flexural capacity that was lower than the needed capacity.

Steel plates and SIFCON were two alternative retrofitting techniques that were used on the beams. Then, while measuring the load, deflection, and stresses, the beams were put through a four-point loading test until they failed.

In comparison to the other retrofitting schemes, the study's findings demonstrated that the SIFCON retrofitting scheme delivered the most noticeable increase in load-carrying capability. The SIFCON-retrofitted beams demonstrated a considerable improvement in the load-carrying capacity as well as in load-deflection behavior and failure mode. In comparison to other retrofitting approaches, the SIFCON-retrofitted beams displayed greater ductility and strain capacity, according to the authors.

The load-carrying capacity of the SIFCON-retrofitted beams increased by up to 122%, according to the authors, while the deflection at failure increased by up to 150%. The rupture strains of the SIFCON-retrofitted beams were up to three times higher than those of the other retrofitting systems, according to the authors. The SIFCON-retrofitted beams also displayed a more ductile failure mode, according to the researchers, with a larger strain capacity and lower stiffness degradation.

Mustaqqim et al. (2016) did an experimental study of slurry-infiltrated fiber-reinforced concrete beams. The beams were tested for flexural strength and the relationship between loads versus deflection was displayed graphically. 19.34 MPa with a 2% volume fraction of steel fiber was the highest flexural strength obtained in this research. The results showed that the flexural strengths and deflections of the prisms with size

25 mm × 100 mm × 500 mm were higher than the prisms which had a steel wire mesh of 50 mm × 100 mm × 500 mm in size. In addition, the highest strength was obtained using the maximum content of 2% by volume fraction of hooked-end steel fibers with an aspect ratio of 67. The highest deflection value was obtained for the same fiber volume fraction content.

Shakir et al. (2018) studied the flexural behavior of slurry-infiltrated fiber concrete beams (SIFCON) containing supplementary cementitious materials. The flexural strength and toughness characteristics were obtained by testing specimens of 100 mm × 100 mm × 400 mm beams at 7 and 28 days. The results attained from these tests were compared to those of the conventional fiber-reinforced mortar (FRM) with 2% fiber content. The test results show superior characteristics of SIFCON to the normal FRM. The use of cementitious materials silica fume (SF) as a partial replacement by weight of cement and the increase in the volume fraction of steel fiber were positive influences. At 28 days, the flexural strength and toughness reached (28.08 MPa) and (159 N.mm), respectively. The study showed that the flexural strength and toughness of SIFCON specimens increase as the volume fraction of steel fiber increases. The increase in volume fraction from (2% to 11%) increases the flexural strength and toughness of SIFCON to 149% and 204%, respectively.

5.3.2 THEORETICAL SIFCON RETROFIT LITERATURE REVIEW

In addition to experimental studies, minimal numerical studies have also been conducted to investigate the behavior of SIFCON-retrofitted concrete beams. For instance, Zhao et al. (2014) created a finite element model to simulate the behavior of

reinforced concrete beams retrofitted with SIFCON under flexural loading. The use of SIFCON, according to the authors, significantly enhanced the structural behavior of the beams compared to unretrofitted beams, for it produced a considerable improvement in ductility and load-carrying capacity. They also noticed that the retrofitted beams' failure mode had changed from a sudden, brittle failure to one that was more ductile and had improved warning behavior. The usefulness of SIFCON as a retrofitting material for reinforced concrete beams was confirmed by the finite element analysis results, which were in good accordance with the experimental findings published in earlier investigations.

Overall, the use of SIFCON has had significant potential for strengthening and retrofitting existing concrete beams. However, more investigation is required to determine the long-term performance and durability of SIFCON-retrofitted concrete beams under a range of loadings and environmental variables.

As recognized from the above literature review a comparative flexural study between concrete beams retrofitted with GFRP, CFRP, FRC, and SIFCON is needed. No literature review was found on the subject of theoretical modeling of FRC and SIFCON. The retrofitted concrete beams with the well-known FRP composite will be compared to concrete beams retrofitted with cementitious composites. This flexural response study of retrofitted beams will determine which retrofit is suitable for the most suitable load application.

6. EXPERIMENTAL PROGRAM

The experimental work was executed in the Civil Engineering Laboratory at Notre Dame University – Louaize. Three LVDTs were calibrated and installed to record the beam deformation and stroke control. Two LVDTs were mounted on both ends of the beam to measure the beam deformation; the third LVDT was set on the moving piston to read the stroke control. The testing compressive MATEST machine used in the research is displayed in Figure 6.1. The loading rate used throughout the experiments was 1mm/min after referring to the American Society for Testing and Materials (ASTM C78). The beam sample is supported on roller bearings, as shown in Figure 6.2. The load is transferred to the specimen through a spreader beam acting as a line load, as shown in Figure 6.3, and loaded until failure. Deformations were recorded and the test results were exported for further analysis and comparison.

Figure 6. 1 - MATEST Testing Machine

Figure 6. 2 - Specimen Supported on Roller Bearings

Figure 6. 3 - Spreader Beam for Loading

6.1 MATERIAL PROPERTIES

Forty-two beams were cast having an identical concrete mix and then retrofitted with different composite materials. Tests were conducted on concrete beams retrofitted with Polymers (CFRP SCH 41, CFRP 11 UP, GFRP SEH 51) and Fiber Cementitious Composites (FRC, SIFCON parallel, and SIFCON perpendicular), in addition to regular control concrete beams, reinforced and non-reinforced for comparison. Each type had three non-reinforced beams and three other reinforced beams with three stainless steel reinforcing bars having a 4 mm diameter.

Hence, the forty-two casted beams were as follows:

- Non-steel reinforced concrete beams retrofitted with:
    - CFRP SCH 41 (3 samples)
    - CFRP 11 UP (3 samples)
    - GFRP SEH 51 (3 samples)
    - FRC (3 samples)
    - SIFCON parallel (3 samples)
    - SIFCON perpendicular (3 samples)

- Steel reinforced concrete beams retrofitted with:
    - CFRP SCH 41 (3 samples)
    - CFRP 11 UP (3 samples)
    - GFRP SEH 51 (3 samples)
    - FRC (3 samples)
    - SIFCON parallel (3 samples)

    - SIFCON perpendicular (3 samples)

- Concrete beam non-steel reinforced (3 samples)
- Concrete beam steel reinforced (3 samples)

Three tests of every composite material were accomplished to verify the results and minimize errors, all graph results are shown in APPENDIX I. Following the ASTM D5045-14 specimen size specifications of ($Length = 4 \times Width$), the specimen size was chosen to be 120 mm × 120 mm × 500 mm as shown in Figure 6.4.

Figure 6. 4 - Wood Formwork

6.1.1 FIBER REINFORCED POLYMERS

FRP composites are composed of short fibers of carbon, glass, etc., which provide a distinctive structural property after being bonded with a resin matrix. Tyfo® SEH-51A, Tyfo® SCH-11UP, and Tyfo® SCH-41 materials were used in this study.

The mechanical properties of Tyfo® SCH-11UP, Tyfo® SCH-41; carbon fiber and Tyfo® SEH-51A; glass fiber materials in addition to the resin Tyfo® S Epoxy used are presented in Fyfe Europe data sheet. Figures 6.5 and 6.6 show carbon and glass fiber polymer sheets, respectively.

Figure 6. 5 - Carbon fiber polymer sheet

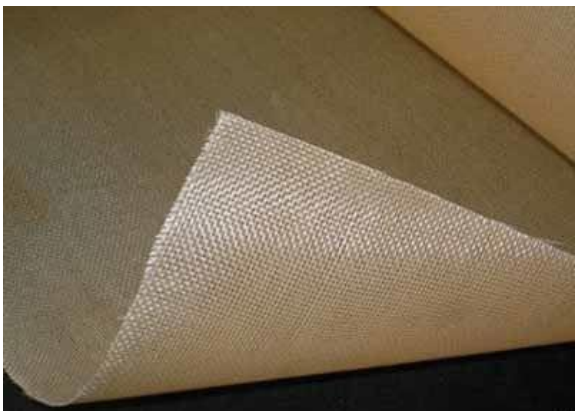

Figure 6. 6 - Glass fiber polymer sheet

6.1.2 FIBROUS CEMENTITIOUS COMPOSITES

In the case of FRC, the composites are made up of 2% by volume of randomly oriented steel fibers intermixed with concrete, or SIFCON with perfectly aligned 12% fiber volume fraction fibers infiltrated with a slurry mix. Those steel fibers are 1 mm in diameter, having an aspect ratio (ratio of length to diameter) of 50, resulting in a valuable change in the mechanical properties of concrete. The fiber's tensile strength is 760 MPa. Figures 6.7 and 6.8 show a 50 mm long hooked-ended steel fiber and the slurry infiltrated fiber concrete mix, respectively.

Figure 6. 7 - 50 mm long Hooked-ended Fiber

Figure 6. 8 - Slurry Infiltrated Fiber Concrete Mix

6.1.3 STEEL REINFORCEMENT

Stainless steel reinforcement was used in the study, with

- D = 4 mm (Bar diameter)
- L = 50 cm (Bar length)
- Yield Strength = 500 MPa
- Modulus of Elasticity = 5,000 MPa

In this study, we utilized steel reinforcement products from ANBAO Corp. (33 Qinhuangxi Street, Quihuangdao, P.R. China 066000).

Three bars with a 2 cm concrete cover were placed at the bottom face of each steel-reinforced concrete specimen. Figure 6.9 displays a sample of the 4 mm diameter stainless steel bars that were used during the experimental testing.

Figure 6. 9 - 4 mm diameter stainless steel reinforcement bars

6.2 TASKS & METHODOLOGY

This section presents the material sampling and mix design proportions used in the investigation, in addition to the casting process.

6.2.1 REGULAR CONCRETE

The regular concrete mix design is identical for the principal concrete beams being retrofitted and the control specimens. For comparison purposes, a consistent concrete strength of $f_c' = 20\ MPa$ was set for all samples. The concrete specimens contained Type I Portland cement, 19 mm (3/4 in.) coarse aggregate, fine aggregate (sand), and water in the proportions of 1: 2: 2: 0.4 by weight, respectively.

Concrete Mix for one beam specimen (Weight Method):

$V_{specimen} = 0.12 \times 0.12 \times 0.5 = 0.0072\ m^3$

Unit weight of concrete: $2400\ kg/m^3$

$\rightarrow W_{concrete} = V_{specimen} \times 2400 = 18\ kg$

Concrete weight was calculated:

$$W_{concrete} = W_{cement} + W_{stone} + W_{sand} + W_{water}$$

Where:

- $V_{specimen}$: Volume of specimen
- $W_{concrete}$: Weight of concrete specimen
- W_{cement}: Weight of cement

- W_{stone}: Weight of stone
- W_{sand}: Weight of sand
- W_{water}: Weight of water

After substituting each weight with its portion, we get the final equation used to pour the beams:

$$W_{concrete} = W_{cement} + 2\,W_{stone} + 2\,W_{sand} + 0.4\,W_{water}$$

$$18\,kg = 5.4\,W_{cement} \rightarrow W_{cement} = 3.33kg$$

Table 6. 1 - Concrete mix proportion by weight for one beam specimen

Material	Proportions by weight	Weight (Kg)
Cement	1	3.33
Sand	2	6.67
Stone	2	6.67
Water	0.4	1.33

After mixing, concrete is poured into the forms and then vibrated to settle and force the entrapped air out of the concrete, as shown in Figure 6.10. For FRC and SIFCON, a steel mesh was placed on the concrete surface to obtain a rough surface for better bonding, as shown in Figure 6.11. The mesh was removed after a couple of days.

Figure 6. 10 - Concrete Beams Freshly poured

Figure 6. 11 - Steel mesh used to roughen the surface

After immersing the concrete beams in water to cure for 28 days, as shown in Figure 6.12, the composite materials were added. FRP sheets were attached to the concrete beams using Sika Fix glue imported from the USA, whereas for FRC and SIFCON, a layer of bonding agent, shown in Figure 6.13, was painted on the rough surface.

Figure 6. 12 - Curing Basin

Figure 6. 13 - Bonding agent used in the retrofitting process of FRC and SIFCON

6.2.2 FIBER REINFORCED POLYMERS

Three types of FRP will be studied, including Carbon SCH 41, Carbon11 UP, and GFRP Glass SEH 51. One layer of FRP sheets was attached to the bottom surface of the concrete beams using the Sika Fix glue. 18 FRP retrofitted beams in total that are composed of non-reinforced and reinforced steel bars at the bottom were tested. Figures 6.14, 6.15, and 6.16 show samples of each type.

Figure 6. 14 - SEH 51 Beam Sample

Figure 6. 15 - SCH 41 Beam Sample

Figure 6. 16 - 11 UP Beam Sample

6.2.3 FIBROUS CEMENTITIOUS COMPOSITES

Three forms of fibrous cementitious composites will be studied, including FRC, SIFCON parallel, and SIFCON perpendicular.

To study the flexural response of beams retrofitted with FRC, the FRC mix in Table 6.2 was used and the mix is displayed in Figure 6.17. A 2% fiber volume is the maximum percent of fibers that can be used in the concrete mixture, avoiding the fiber balling effect resulting from studies conducted by Lee et.al (1987) and Naaman et.al (1989). Hence, a 2% fiber volume fraction was used in the FRC mix for investigation. Every mold included the formwork of 6 beam specimens. The same formwork of the concrete beams was elevated 25 mm above the ground, as shown in Figure 6.18, and then FRC was added to the previously cast concrete, as shown in Figure 6.19. The thickness of the composite is 2.5 cm. A sample concrete beam with hardened FRC is shown in Figure 6.20.

Table 6. 2 - FRC Quantities Sheet

FRC	Cement	Sand	Aggregates (Ø=3/4)	Water	Super plasticizer	Fibers
Proportions	1	1.5	2.5	0.5	0.015	2% (by volume)
Quantity in Kg/ Mold	3.92	5.88	9.8	1.96	0.0588	1.4

Figure 6. 17 - FRC Mix

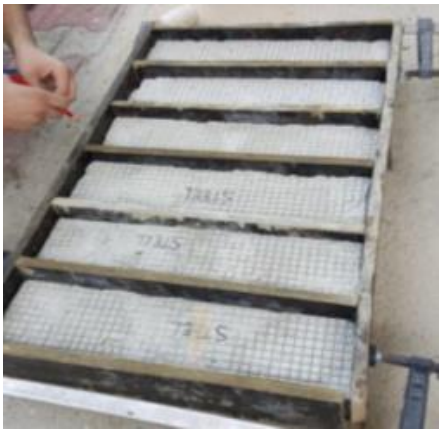

Figure 6. 18 - Elevated Formwork

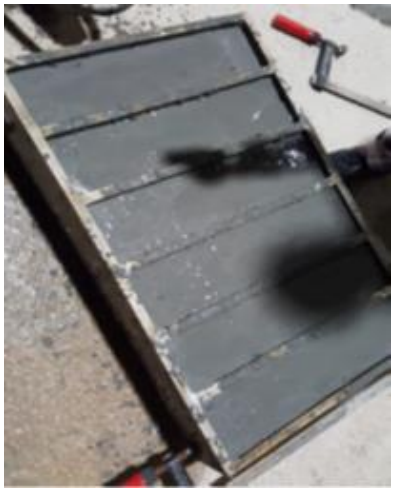

Figure 6. 19 - FRC Mix added to the Specimens

Figure 6. 20 - Concrete Specimen with FRC Hardened

To study the flexural response of beams retrofitted with SIFCON, the SIFCON mix in Table 6.3 was used. A study by Naaman et.al on stress-strain properties of SIFCON showed that a 12% hooked steel fiber produces the maximum tensile strength. Based on that, a 12% fiber volume fraction was used in this study. The proportions of the mix were used by Krstulovic and Malak (2019) in their study on the tensile properties of slurry-infiltrated mat concrete (SIMCON). The same formwork was also elevated 25 mm above the ground for the SIFCON placed parallel and perpendicular. Figure 6.21 shows the SIFCON fibers that are placed parallel to the longest side of the form. Whereas, in Figure 6.22, SIFCON fibers are placed perpendicular to the longest side of the form. The SIFCON fibers are directly laid in the formwork before casting and

pouring the mix demonstrated in Table 6.3. In addition, the forms were fixed at the edges to prevent the high slurry mix from leaking outside the forms. Every mold included the formwork of 6 beam specimens.

Table 6. 3 - SIFCON Quantities Sheet

SIFCON	Cement	Silica Sand	Micro Silica	Water	Super plasticizer	Fibers
Proportions	1	0.6	0.3	0.3	0.045	12% (by volume)
Quantity in Kg/ Mold	7.06	4.24	2.12	2.12	0.32	8.4

Figure 6. 21 - Elevated Formwork with SIFCON placed parallel

Figure 6. 22 - Elevated Formwork with SIFCON placed perpendicular

The formwork was covered the next day of casting using a sheet textile shown in Figure 6.23, which is water absorbent for humidification before curing. Figure 6.24 shows the fresh hardened SIFCON after removing the forms. The specimens were subjected to 28 additional days of curing after retrofitting them with FRC and SIFCON.

Figure 6. 23 - Water Absorbent Textile

Figure 6. 24 - Concrete Specimens Retrofitted with SIFCON

6.3 EXPERIMENTAL RESULTS AND DISCUSSION

Four figures and two tables provide data to interpret and compare the experimental comparison of polymers and cementitious composites with and without steel. Figure 6.25 shows the experimental comparison of polymers without steel and with steel, while Figure 6.26 shows the experimental comparison of cementitious composites without steel and with steel. Figures 6.27 and 6.28, on the other hand, provide an experimental comparison of cementitious composites and polymers without and with steel, respectively. The experimental results for polymers and cementitious composites without steel are shown in Table 6.4, whereas those for polymers and cementitious composites with steel are shown in Table 6.5. The performance of polymers and cementitious composites with and without steel in various applications can be analyzed using these figures and tables. The testing results display the effect of composites and steel reinforcements on beam specimens, in which every combination results in a unique response.

The succeeding data utilize various parameters related to the testing and analysis of concrete, steel reinforcement, and retrofitting composites. The symbols used in this section include E_c for the modulus of elasticity of concrete and E_y for the modulus of elasticity of the system at yield. Deformation at first crack, yield, and ultimate are represented by Δ_{cr}, Δ_y, and Δ_u, respectively. Loads at first crack, yield, and ultimate are represented by P_{cr}, P_y, and P_u, respectively. When the system has a composite and steel reinforcement, then we have Δ_{r1} and Δ_{r2}. Where Δ_{r1} and Δ_{r2} represent the deformations at the rupture of the composite with steel still existing and at the failure of the total system with the rupture of steel reinforcement, respectively. Loads at Δ_{r1} and Δ_{r2} are

represented by $P_{r1,}$ and P_{r2}, respectively. When the system has a composite without steel reinforcement, then we have $\Delta_{r2\ No\ Steel}$. Where $\Delta_{r2\ No\ Steel}$ represents the deformation at the rupture of the composite and total failure of the system. Load at $\Delta_{r2\ No\ Steel}$ is represented by $P_{r2\ No\ Steel}$.

Other parameters used in this section include K_c for stiffness of concrete, K_y for stiffness of the system at yield, and μ for ductility ratio. Additionally, the gross moment of inertia and cracked moment of inertia are represented by I_c and I_y, respectively.

The parameters are calculated using the following equations:

- Stiffness of concrete: $K_c = \frac{P_{cr}}{\Delta_{cr}}$ $Eq.(6.1)$
- Modulus of elasticity of concrete: $E_c = \frac{K_c L^3}{48 I_c}$ $Eq.(6.2)$
- Stiffness of the system at yield: $K_y = \frac{P_y - P_{cr}}{\Delta_y - \Delta_{cr}}$ $Eq.(6.3)$
- Modulus of elasticity of the system at yield: $E_y = \frac{K_y L^3}{48 I_y}$ $Eq.(6.4)$
- Ductility ratio:
    - Without steel reinforcement: $\mu = \frac{\Delta_{r2\ No\ Steel}}{\Delta_y}$ $Eq.(6.5)$
    - With steel reinforcement: $\mu = \frac{\Delta_{r1}}{\Delta_y}$ $Eq.(6.6)$

Where μ is calculated at the rupture of the composite.

T refers to the toughness of the system, which is a measure of a material's ability to absorb energy before breaking. $T_{concrete}$ is the toughness of a normal concrete specimen and TI denotes to the toughness index, where it is calculated by the following equation:

$$TI = \frac{T}{T_{Concrete}} \qquad Eq.(6.7)$$

We can observe in Figure 6.25 and Tables 6.4 and 6.5 all three polymers examined with and without steel reinforcement. The graphs in Figure 6.25 can clearly show and compare the effect of steel when introduced to the concrete specimen. The Carbon SCH 41 with steel graph shows a shift to the right with respect to the Carbon SCH 41 without steel graph, in which the ductility ratio increases by around 218%. P_y increased from 21.35 kN to 22.93 kN and the P_u increased from 50.33 kN to 52.19 kN with a 66% increase in Δ_U. K_y also showed a significant increase from 39.26 kN/mm to 52.75 kN/mm and the E_y showed a 33.1% increase. The toughness (T) of the specimen as well increased from 50.49 kN-mm to 214.27 kN-mm.

When steel reinforcement was introduced to Carbon 11 UP composite, the ultimate load capacity increased from 39.3 kN to 46.19 kN with a slight decrease in the ultimate delta, as shown in Figure 6.25 and Tables 6.4 and 6.5. The ductility ratio clearly shows a remarkable increase of around 86%. The yield strength increased from 20.14 kN to 22.05 kN and the ultimate strength increased from 39.30 kN to 46.19 kN with a slight decrease in the ultimate delta. Stiffness (K_y) also indicated a significant increase from 24 kN/mm to 50.34 kN/mm and the modulus of elasticity showed a 106% increase. In addition, the toughness of the specimen increased from 42.27 kN-mm to 112.72 kN-mm.

In addition, Glass SEH 51 without steel reinforcement had a higher ultimate load capacity than with steel of around 22.5%. The ductility ratio increased by around 181% and the yield strength increased from 18.61 kN to 21.95 kN. Δ_{R1} of the steel-reinforced specimen significantly increased compared to the specimen without steel reinforcement. Elastic Stiffness (K_y) as well showed a major increase from 30.27 kN/mm to 46.19 kN/mm and the modulus of elasticity showed a 48.7% increase. Plus,

the toughness of the steel-reinforced Glass SEH 51 specimen was recorded to be 121.55 kN-mm compared to 44.56 kN-mm of the non-reinforced Glass SEH 51 specimen.

The above results allow us to indicate the effect of steel reinforcement, which develops a more ductile behavior for the samples. Steel reinforcement enhances the capability in sustaining higher loads for Carbon SCH 41 and Carbon 11 UP specimens. All three composites show a major increase in the stiffness (K_y), modulus of elasticity, and toughness after steel reinforcement was introduced to the system. In addition, Carbon SCH 41 has the highest load capacity among the polymers with and without steel reinforcement. The strength of those tested steel-reinforced samples did not suddenly drop as the specimens without steel reinforcement, but a smoother variation in the load capacity took place after reaching peak values.

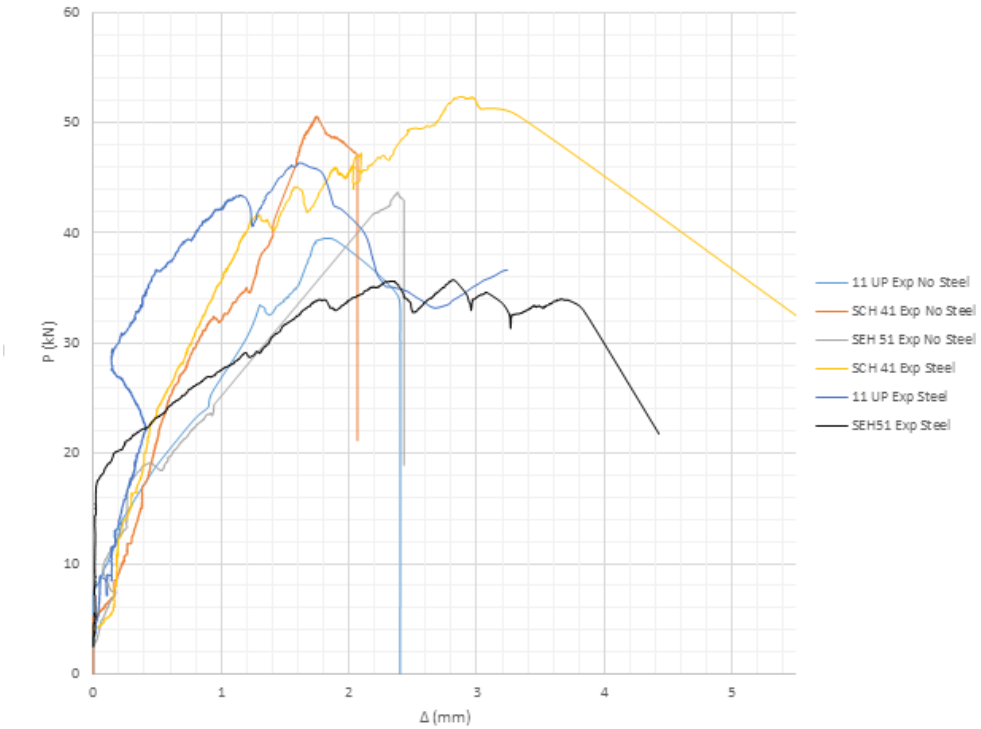

Figure 6. 25 - Polymers without and with steel experimental comparison

Table 6. 4 - Experimental results of polymers and cementitious composites without steel

	Without Steel																
	Δcr	Pcr	Δy	Py	Δ_U	P_U	Δ_{R1}	P_{R1}	Δ_{R2}	P_{R2}	μ	Stiffness Ky	Ey	Stiffness Kc	Ec	T	TI
	mm	kN	mm	kN	mm	kN	mm	kN	mm	kN		kN/mm	kN/mm2	kN/mm	kN/mm2	kN-mm	
Regular Concrete	0.10	5.83	0.29	8.19	0.42	9.04	-	-	0.42	0.00	1.45	12.50	1.88	57.73	8.70	2.70	1.00
GLASS SEH - 51	0.17	7.16	0.55	18.61	2.39	43.54	-	-	2.43	0.00	4.43	30.27	31.71	41.89	6.31	44.56	16.48
CARBON 11 - UP	0.07	8.19	0.57	20.14	1.75	39.30	-	-	2.40	0.00	4.21	24.00	16.82	113.69	17.13	42.27	15.63
CARBON SCH - 41	0.17	8.00	0.51	21.35	1.76	50.33	-	-	2.07	0.00	4.08	39.26	19.25	48.19	7.26	50.49	18.67
FRC	0.05	4.97	0.06	8.45	0.22	25.54	-	-	0.69	2.80	11.19	348.00	27.47	95.58	14.40	3.70	1.37
SIFCON Parallel	0.07	6.19	-	-	1.78	47.67	-	-	7.61	1.20	113.58	23.45	2.27	92.36	13.92	40.54	14.99
SIFCON Perpendicular	0.07	5.90	-	-	0.46	19.51	-	-	2.70	3.57	40.30	43.20	3.84	88.10	13.28	5.21	1.93

Table 6. 5 - Experimental results of polymers and cementitious composites with steel

	With Steel																
	Δcr	Pcr	Δy	Py	Δ_U	P_U	Δ_{R1}	P_{R1}	Δ_{R2}	P_{R2}	μ	Stiffness Ky	Ey	Stiffness Kc	Ec	T	TI
	mm	kN	mm	kN	mm	kN	mm	kN	mm	kN		kN/mm	kN/mm2	kN/mm	kN/mm2	kN-mm	
Regular Concrete	0.09	1.33	0.34	5.19	0.51	7.53	-	-	0.82	5.11	2.40	15.55	23.43	14.34	21.62	5.13	1.00
GLASS SEH - 51	0.07	8.56	0.36	21.95	2.84	35.54	4.43	21.77	15.31	0.00	12.43	46.19	47.15	129.67	19.54	121.55	23.70
CARBON 11 - UP	0.15	8.61	0.41	22.05	1.66	46.19	3.24	36.65	15.10	0.00	7.86	50.34	34.72	59.34	8.94	112.72	21.98
CARBON SCH - 41	0.14	7.21	0.44	22.93	2.92	52.19	5.73	30.61	15.30	0.00	12.98	52.75	25.62	50.42	7.60	214.27	41.78
FRC	0.05	6.36	0.07	9.70	0.20	29.05	8.10	3.51	15.12	0.00	124.62	257.31	20.29	122.23	18.42	5.31	1.03
SIFCON Parallel	0.06	7.61	-	-	1.60	58.42	8.05	7.02	15.10	0.00	129.84	36.20	3.55	122.81	18.51	262.04	51.09
SIFCON Perpendicular	0.07	5.74	-	-	1.04	28.80	7.98	3.87	15.20	0.00	120.91	30.81	2.81	86.89	13.10	130.37	25.42

Figure 6.26 and Tables 6.4 and 6.5 show the cementitious composites compared to one another without and with steel reinforcement. FRC without steel had an ultimate load capacity of 25.54 kN and reached 29.05 kN after the introduction of steel reinforcement into the specimen, resulting in a 12% increase. The ductility ratio of the FRC specimen largely increased from around 11.19 to 124.62. The specimen's toughness improved from 3.70 kN-mm to 5.31 kN-mm, with a total of 43.5% increase. A major decrease in the stiffness (K_y) was recorded from 348 kN/mm to 257.31 kN/mm and the modulus of elasticity showed a 35.4% decrease.

In addition, Figure 6.26 and Tables 6.4 and 6.5 indicated that SIFCON parallel with steel reinforcement had a higher ultimate load capacity than without steel of around 22.54%, with 58.416 kN compared to 47.67 kN, respectively. However, the ductility ratio decreased to around 12.42%. Δ_{R1} of the steel-reinforced specimen significantly increased compared to the specimen without steel reinforcement. Stiffness (K_y) as well showed a major increase from 23.45 kN/mm to 36.2 kN/mm and the modulus of

elasticity showed a 56.4% increase. Moreover, the toughness of the steel-reinforced SIFCON parallel specimen was noted to be 262.04 kN-mm compared to 40.54 kN-mm of the non-reinforced Glass SEH 51 specimen.

SIFCON perpendicular showed in Figure 6.26 and Tables 6.4 and 6.5 a considerable increase in the maximum load capacity, for it increased from 19.51 kN to 28.80 kN with an approximately 47.62% growth. A significant increase in the ultimate delta of approximately 125.5% and the ductility ratio increased by around 200%. Stiffness (K_y) indicated a slight decrease from 40.30 kN/mm to 30.81 kN/mm and the modulus of elasticity showed a 36.65% decrease. Furthermore, a major increase in the toughness of the specimen was noted, from 5.21 kN-mm to 130.37 kN-mm. Steel reinforcement had a significant role in SIFCON perpendicular composite, in which the graphs shifted to the right and the specimens became more ductile.

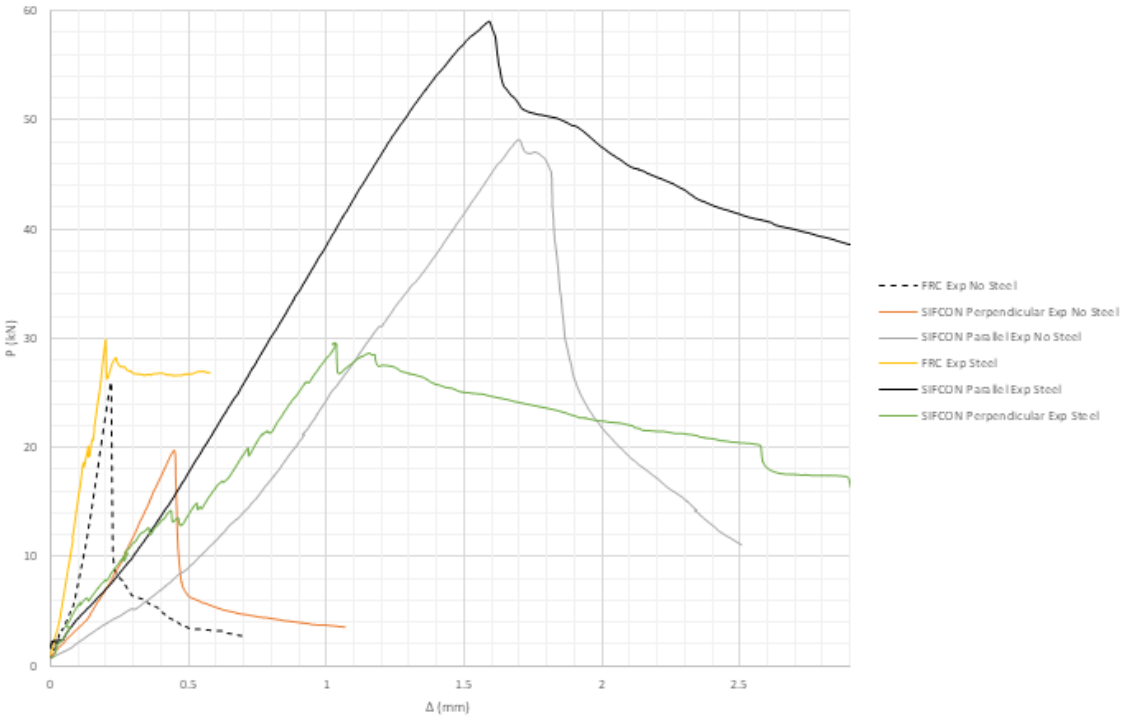

Figure 6. 26 - Cementitious composites without and with steel experimental comparison

The introduction of steel reinforcement led to an enhancement of the ability in sustaining higher loads for all three cementitious composites, where SIFCON parallel controlled the highest load capacities without and with steel reinforcement among all the cementitious composites. The above outcomes indicate the major effect of steel reinforcement in specimens on their behavior, in which steel reinforcement boosted the toughness of all three cementitious composites after being introduced to the system.

Polymers and cementitious composites without steel reinforcement are compared in Table 6.4 and plotted in Figure 6.27. We notice that polymers mainly govern the highest loads from around 40 to $50\ kN$ as well as SIFCON parallel with $Pu = 47.67\ kN$. However, we can realize that polymers tend to have a sudden failure directly after peak loads, while cementitious composites can sustain a considerable amount of strength after peak levels with respect to polymers. This can be directly detected from the sudden drop of polymer graphs and a smoother variation was observed for cementitious composites. Cementitious composites result in a large ductility ratio compared to polymers, for the average ductility ratio for polymers is around 4.24 compared to 66 for cementitious composites. In addition, the stiffnesses of Carbon 11 UP and SIFCON parallel are the least stiff among all composites without steel reinforcement with approximately 24 kN/mm. Polymers and SIFCON parallel govern the highest toughness outcomes from around 40 to 50 kN-mm.

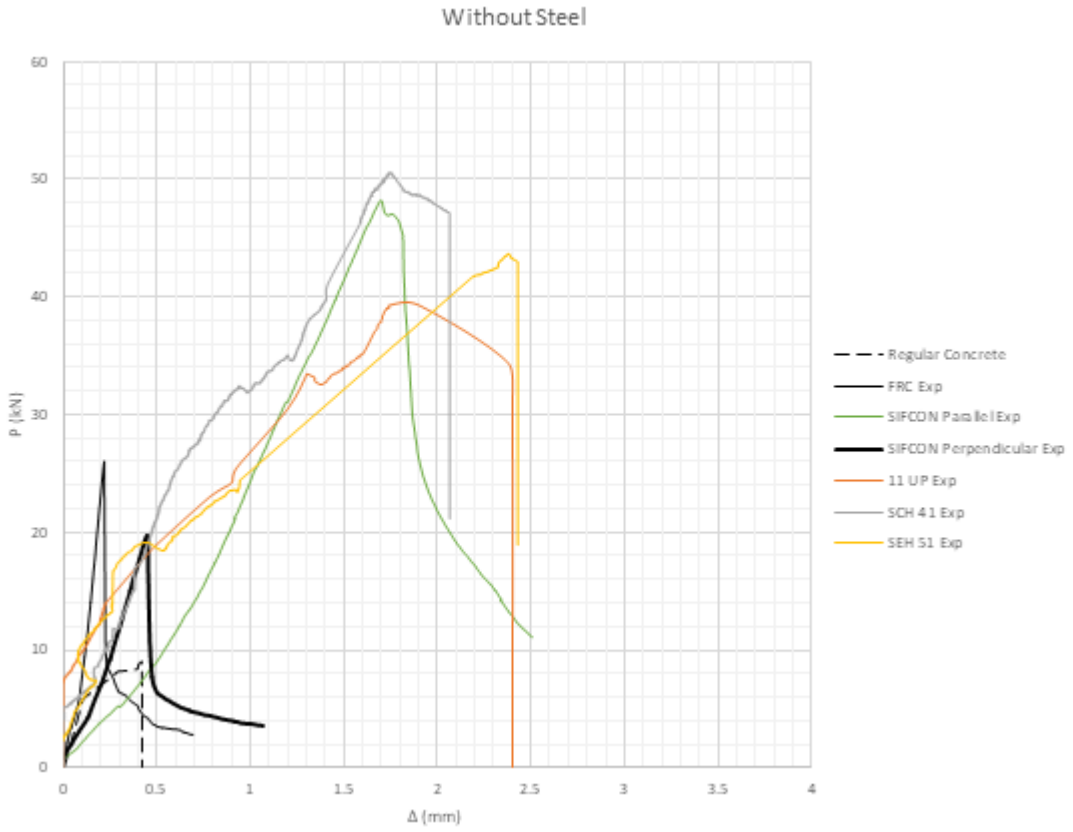

Figure 6. 27 - Polymers & Cementitious composites without steel experimental comparison

Table 6.5 and Figure 6.28 compare the experimental data of polymers and cementitious composites with steel reinforcement. SIFCON parallel reached the highest load capacity of 58.416 kN among all steel-reinforced specimens and SIFCON perpendicular had the lowest ultimate load capacity of 28.80 kN, excluding regular concrete. This indicates the importance of the direction of steel fibers being placed in SIFCON specimens, for it can reach the highest or lowest load capacities with a simple direction modification. In addition, the SIFCON parallel has the highest toughness index, having the largest area under the curve. Cementitious composites result in a large ductility ratio compared to polymers, resulting in an average ductility ratio for polymers around 11.1, compared to 125.1 for cementitious composites.

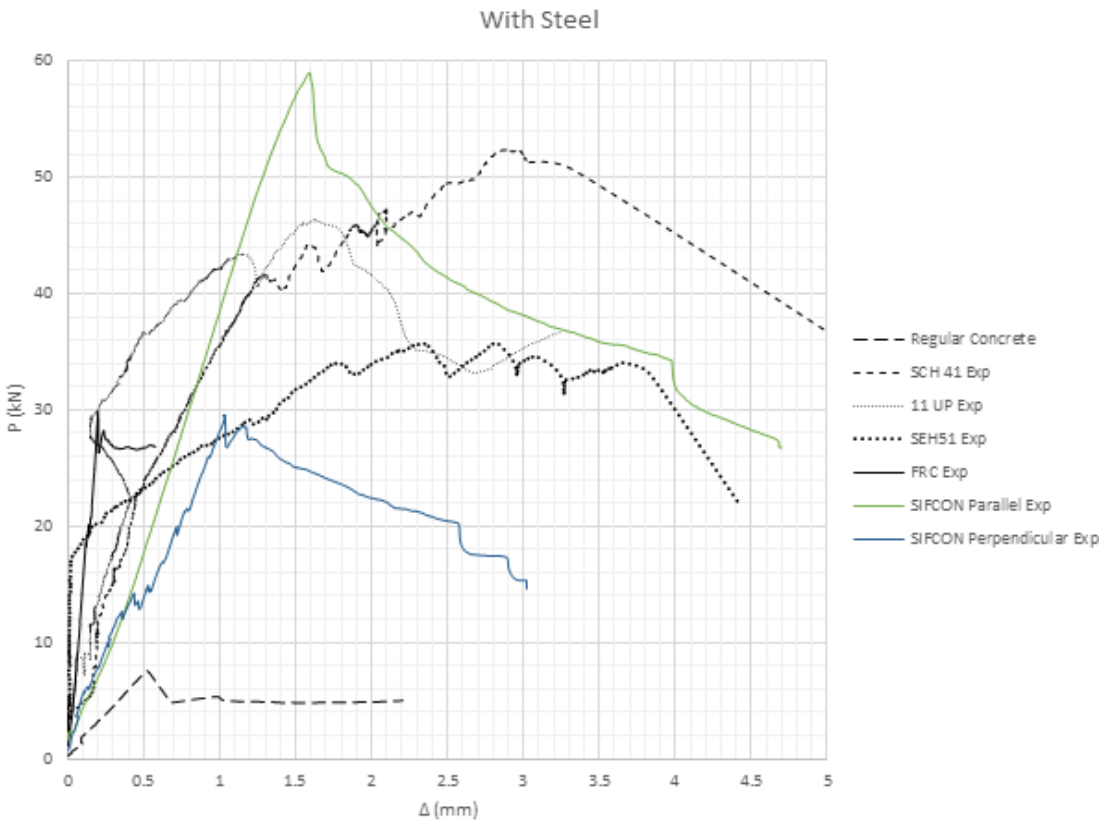

Figure 6. 28 - Polymers & Cementitious composites with steel experimental comparison

Specimen Failure:

FRP**:**

After the specimen retrofitted with FRP is loaded, bending takes place and the separation occurs between the concrete and the FRP sheet, known as the delamination, as shown in Figures 6.29 and 6.30 for carbon and glass polymers. No rupture for the sheets was observed.

Figure 6. 29 - Failure of Concrete Specimens Retrofitted with CFRP SCH 41

Figure 6. 30 - Failure of Concrete Specimens Retrofitted with GFRP SEH 51

FRC:

In the case of FRC retrofits, a single crack occurs at the mid-span at ultimate loads. Once the crack occurs, the load will drop resulting in debonding between the fibers and the matrix. Consequently, the pull-out of the fiber takes place across the crack as shown in Figure 6.31. This behavior is the result due to the random distribution and low fiber volume fraction in FRC composites.

Figure 6. 31 - Failure of Concrete Specimens Retrofitted with FRC

SIFCON perpendicular:

Figure 6.32 displays the failure of SIFCON perpendicular, in which it also exhibits a similar crack behavior phenomena as FRC. However, the performance is improved due to the larger fiber percentage crossing the crack (not necessarily aligned perfectly perpendicular to the longitudinal axis of the beam).

Figure 6. 32 - Failure of Concrete Specimens Retrofitted with SIFCON perpendicular

SIFCON parallel:

The failure of concrete beams retrofitted with SIFCON parallel exhibit a multiple cracking mechanism. A crack takes place in the middle of the beam followed by multiple cracks on either side the initial crack. This effect results in larger load capacity and higher ductility. Following that, the initial crack width increases resulting in higher loads for debonding and pull-out of fibers since the fibers are aligned and interconnected. Thus, higher loads, deflections, and ductility. This phenomenom is as shown in Figure 6.33. Hence, the multiple cracking mechanism leads to a higher

absorption and eventual debonding of a longer interconnected fiber.

Figure 6. 33 - Failure of Concrete Specimens Retrofitted with SIFCON parallel

7. THEORETICAL PROGRAM

7.1 GENERAL MOMENT-CURVATURE AND LOAD-DEFLECTION CURVES

The typical behavior of beams retrofitted with composites with or without steel reinforcement corresponds to different stages of the material's response to the applied load. Figure 7.1 displays the typical load-deflection curve that is obtained from the typical moment-curvature graph shown in Figure 7.2. The response is characterized by the following various zones:

Zone 1: Signifies the first crack of the concrete specimen, denoted by Δ_{cr}, P_{cr}, M_{cr}, and K_c, as defined previously. M_{cr} and ϕ_{cr} represent the moment capacity and curvature at the first crack, respectively. The stiffness K_c and E_cI_c are defined by the slope of the load-deflection and moment-curvature curves, where E_c is the elastic modulus of elasticity of the concrete, and I_c is the gross moment of inertia of the concrete specimen.

Zone 2: Represents the phase in which the whole composite system remains elastic, where one of the material dominates the yielding phase (The phase at which either material reaches yield first). In the proposed research, the limiting elastic stress is of concrete which is around $0.7f'_c$, where f'_c is the compressive strength of concrete. This zone is characterized by Δ_y and P_y, as previously defined. In addition to M_y and ϕ_y that represent the moment capacity and curvature at yield, respectively.

Zone 3: This is the region where the system reaches its ultimate capacity. This zone is characterized by Δ_u and P_u, as previously defined. In addition to M_u and ϕ_u that represent the moment capacity and curvature at ultimate, respectively.

The stiffness K_y is defined by the slope of the load-deflection curve of all the samples between first crack and yield. For SIFCON parallel and perpendicular, the stiffness Ky' is represented by the slope of the line between first crack and ultimate capacity, as shown by the dashed line in Figures 7.1 and 7.2. Thus, in SIFCON there is no yielding phase since the stress strain response in tension of the SIFCON composite has no elastic limit. The slope of the lines EyIy and Ey'Iy' in the moment-curvature responses as shown in Figure 7.2 represent the rotational stiffness accordingly.

At the ultimate point, various scenarios can occur based on the composite used in the specimen. The system achieves its maximum capacity when SIFCON parallel is used. This case the concrete and SIFCON parallel reach their maximum capacities, where the strain of concrete reaches 0.003 and SIFCON reaches its ultimate strain capacity. This is the optimized setup, in which it is the only combination in which it maximizes the capacity of concrete while utilizing the composite's maximum capacity.

In case where FRP is the composite, concrete does not reach its capacity due to the delamination of FRP sheets at this point. FRP and concrete do not reach their maximum capacities.

At the peak point of the system, SIFCON perpendicular and FRC reach their maximum capacities, while concrete doesn't. Hence, the specified combinations do not optimize the system.

Zone 4: This zone displays the failure mode of the system, as a result of the failure of the composite when there is no steel or as a result of the failure of the steel reinforcement followed by the composite.

When the concrete is retrofitted with a composite only, $\Delta_{r2\ No\ Steel}$ represents the final

deflection at failure. In this case, the system follows the dashed line from the peak load at Δ_u to $\Delta_{r2\ No\ Steel}$. This indicates that when the composite fails, the total system directly fails, which happens through delamination of FRP or rupture of the cementitious composites.

When the concrete is retrofitted with a composite and steel reinforcement, Δ_{r1} and P_{r1} represent the condition at which the steel reinforcement remains resisting the load. Δ_{r2} represents the final deflection after failure of the steel reinforcement. This phase is represented as shown in Figure 7.1 by the two segment lines joining Δ_u, Δ_{r1}, and Δ_{r2}. Steel reinforcement retains the system from failing directly after the failure of the composite, for it can provide additional load-carrying capacity and create a more ductile, robust, and durable system.

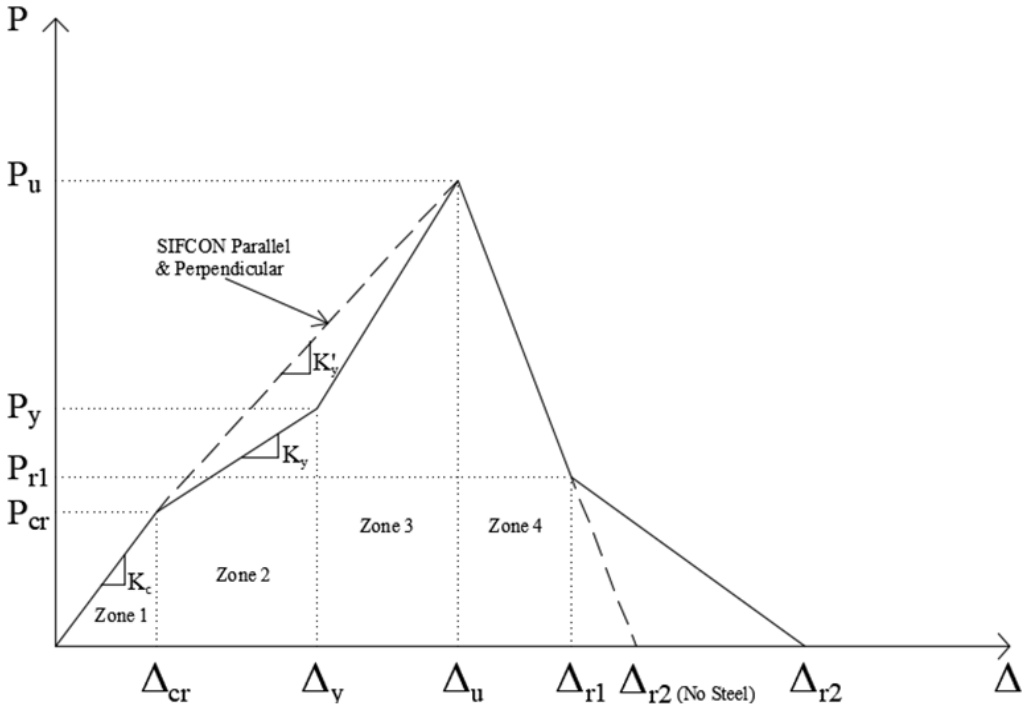

Figure 7. 1 – Load-Deflection diagram of polymers and cementitious composites with and without steel reinforcement

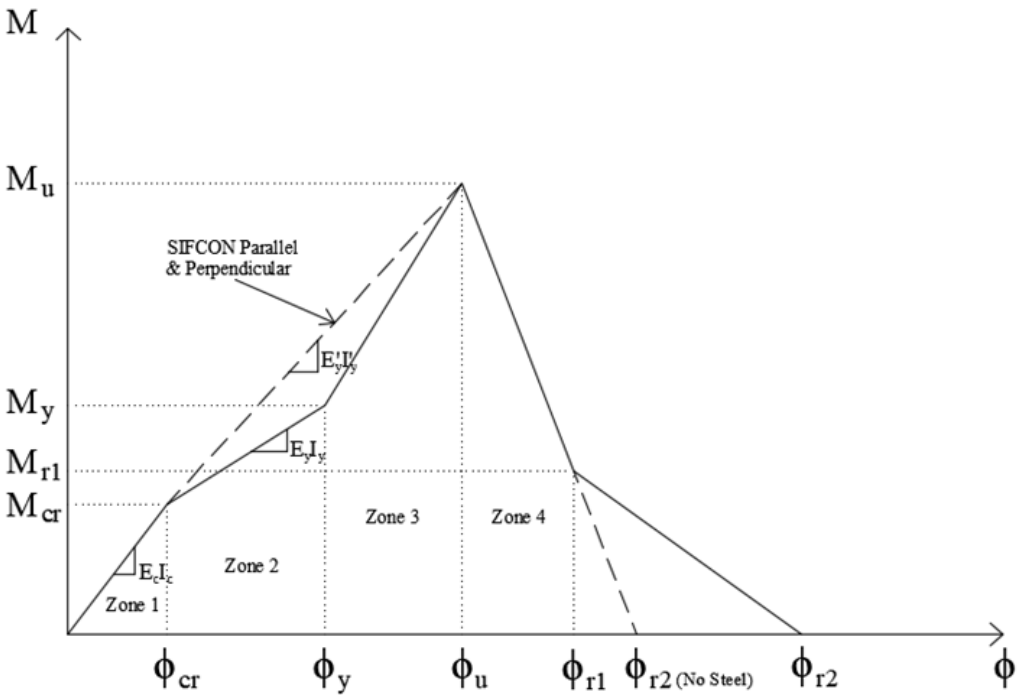

Figure 7. 2 – Moment-Curvature diagram of polymers and cementitious composites with and without steel reinforcement

7.2 MODEL DEVELOPMENT

The following assumptions have been considered in the development of the model:

- The effect of bond strength between the composites and the concrete specimen is neglected in the model.
- The presence of FRC and SIFCON during the first crack of the concrete is neglected because of bonding issues.
- The presence of FRP during the first crack of the concrete is ignored since the thickness of the FRP is negligible compared to the full section of concrete.
- The bonding and debonding of fibers in cementitious composites is ignored in the model.
- The beam sections remain plane after bending occurs.

First Crack Phase

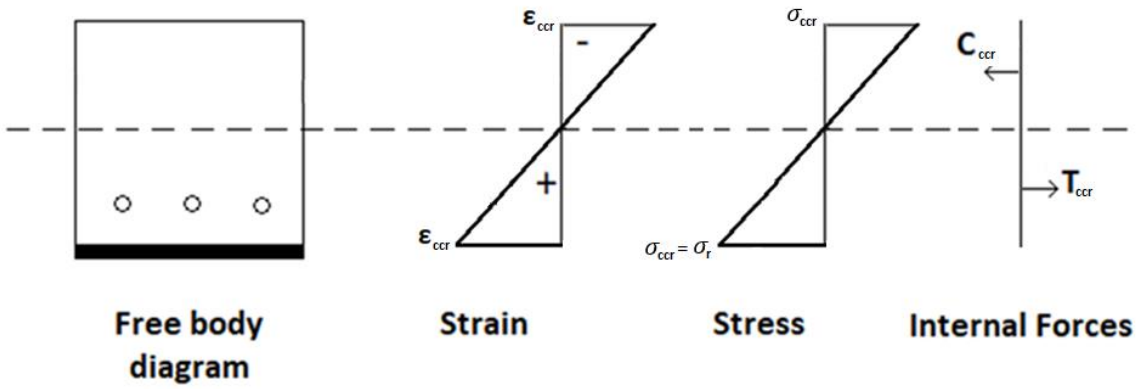

Figure 7. 3 - Bending relationships at first crack with steel reinforcement and retrofitted with a composite

At first crack, the stress in tension at concrete reaches modulus of rupture, as shown in Figure 7.3. The stress-strain diagram is linear and stresses and strains are proportional.

The generalized first crack moment equation is based on the flexural formula since the stresses and strains are linear. Equation 7.1 shows the first cracking moment:

$$M_{cr} = \frac{\sigma_{ccr} \frac{1}{12} b h^3}{\frac{h}{2}} \qquad (Eq. 7.1)$$

$$\text{Where } \sigma_{ccr} = \sigma_r \qquad (Eq. 7.2)$$

σ_r is the concrete's modulus of rupture equal to 3.27 MPa, b is the section width, and h is the section depth. The effect of the steel reinforcement and the effect of the composite material are not taken into consideration, according to the assumptions above.

The applied load can be obtained using the following equation:

$$P_{cr} = M_{cr}\frac{4}{L} \qquad (Eq.7.3)$$

Where L is the length of the beam and all other parameters are as defined previously.

The first crack's deflection (Δ_{cr}) can be obtained from the conjugate beam method in the elastic stage, as shown in equation 7.4:

$$\Delta_{cr} = \frac{1}{2}\emptyset_{cr}\left(\frac{L}{2}\right)^2 - \frac{1}{2}\emptyset_{cr}\left(\frac{L}{2}\right)^2\frac{1}{3} \qquad (Eq.7.4)$$

With $\emptyset_{cr}$ being the crack's curvature, as shown in equation 7.5:

$$\emptyset_{cr} = \frac{\varepsilon_{ccr}}{\frac{h}{2}} = \frac{\sigma_{ccr}}{\frac{h}{2}E_c} \qquad (Eq.7.5)$$

Where ε_{ccr} represents the strain at rupture, E_c is the modulus of concrete, and all other parameters are as defined previously.

Yield Phase

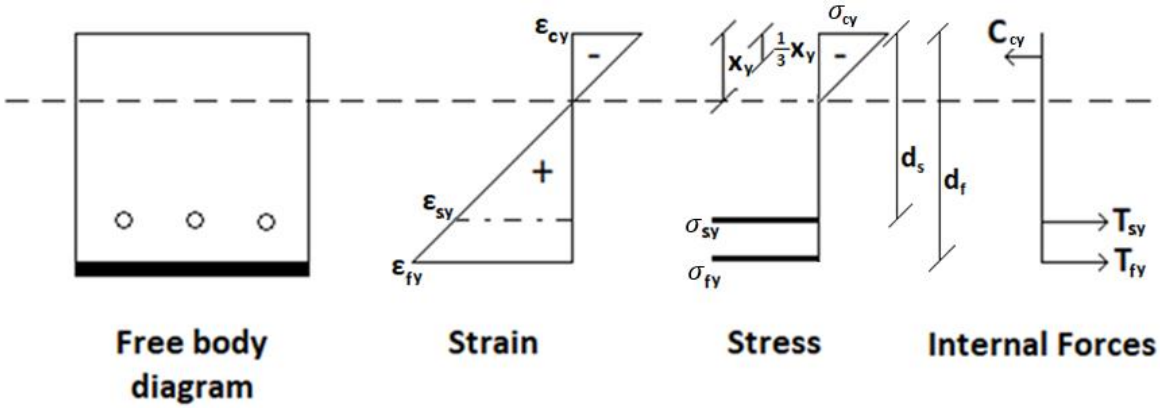

Figure 7. 4 - Bending relationships at yield with steel reinforcement and retrofitted with a composite

This phase is not applicable to the case of beams retrofitted with SIFCON, as explained previously.

As shown in Figure 7.6 and using the force couple method. The neutral axis x_y can be determined by:

$$C_{cy} = T_{sy} + T_{fy} \qquad (Eq. 7.6)$$

Where C_{cy} is the compression force in concrete, T_{sy} is the tension force in the steel reinforcement, and T_{fy} is the tension force in the composite.

The strain in the concrete is obtained by the following two equations:

In the case of FRP: $\varepsilon_{cy} = \frac{0.7\, f_c'}{E_c}$ $\qquad (Eq. 7.7)$

In the case of FRC: $\varepsilon_{cy} = \frac{\varepsilon_{fy} x_y}{(d_f - x_y)}$ $\qquad (Eq. 7.8)$

Where ε_{fy} represents the elastic strain of FRC, d_f is the distance from the composite

centroid to extreme compression fiber, and all other parameters are as defined previously.

The strain in the FRP composite can be determined using similar triangles, as shown in equation 7.9:

$$\varepsilon_{fy} = \frac{\varepsilon_{cy}\,(d_f - x_y)}{x_y} \qquad (Eq.\,7.9)$$

While in the case of FRC, ε_{fy} is the elastic strain of the composite.

The strain in the steel can be determined using similar triangles, as shown in the following equations:

$$\varepsilon_{sy} = \frac{\varepsilon_{cy}\,(d_s - x_y)}{x_y}\ in\ the\ case\ of\ FRP \qquad (Eq.\,7.10)$$

$$\varepsilon_{sy} = \frac{\varepsilon_{fy}(d_s - x_y)}{(d_f - x_y)}\ in\ the\ case\ of\ FRC \qquad (Eq.\,7.11)$$

The stresses in the steel reinforcement, composite, and concrete can be calculated using equations 7.12, 7.13, and 7.14, respectively:

$$\sigma_{sy} = E_s \varepsilon_{sy} \qquad (Eq.\,7.12)$$

$$\sigma_{fy} = E_f \varepsilon_{fy} \qquad (Eq.\,7.13)$$

$$\sigma_{cy} = E_c \varepsilon_{cy} \qquad (Eq.\,7.14)$$

From equation 7.6, the neutral axis can be obtained by:

$$\frac{1}{2}\sigma_{cy} b x_y = \sigma_{fy} A_f + \sigma_{sy} A_s \qquad (Eq. 7.15)$$

Where $A_f = t_f b$ $\qquad (Eq. 7.16)$

The generalized yield moment equation that is based on summing moments about the compression is

$$M_y = \sigma_{fy} A_f \left(d_f - \frac{x_y}{3}\right) + \sigma_{sy} A_s \left(d_s - \frac{x_y}{3}\right) \qquad (Eq. 7.17)$$

Where x_y is the distance from the fiber of maximum strain to the neutral axis, t_f is the thickness of the fiber composite, σ_{fy} is the yield strength of the fiber composite, σ_{sy} is the yield strength of the steel reinforcement, ε_{cy} is the strain in the concrete, ε_{sy} is the strain in the steel reinforcement, ε_{fy} is the strain in the composite, d_s is the distance from the steel reinforcement centroid to extreme compression fiber, A_s is the area of steel reinforcement, and all other parameters are as defined previously.

In case where the system is not reinforced with steel, A_s should be replaced with zero and equations 7.10 and 7.11 are not applicable.

The applied load can be obtained using the following equation:

$$P_y = M_y \frac{4}{L} \qquad (Eq. 7.18)$$

The yield curvature is found using the following equation:

$$\emptyset_y = \frac{\varepsilon_{fy}}{(d_f - x_y)} \qquad (Eq. 7.19)$$

Finally, the yield deflection can be obtained from the conjugate beam method:

$$\Delta_y = \frac{1}{2}\emptyset_y \left(\frac{L}{2}\right)^2 - \frac{1}{2}\emptyset_y \left(\frac{L}{2}\right)^2 \frac{1}{3} \qquad (Eq. 7.20)$$

Ultimate Phase

For SIFCON parallel:

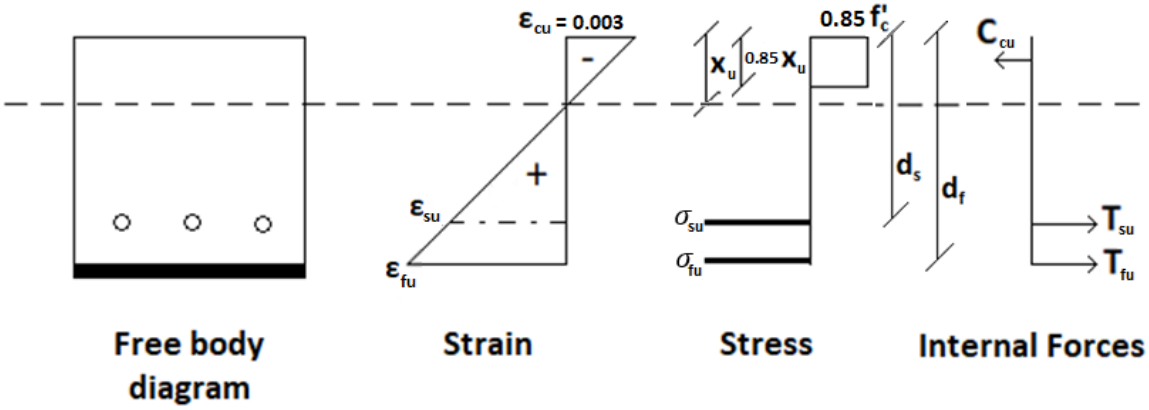

Figure 7. 5 - Bending relationships at ULS with steel reinforcement and retrofitted with SIFCON parallel composite

Wittney block is used since the strain in concrete (ε_{cu}) is 0.003.

Using similar triangles, equations 7.21 and 7.22 determine the strain as a function of x_u in steel reinforcement and SIFCON parallel, respectively.

$$\varepsilon_{su} = \frac{\varepsilon_{cu}\ (d_s - x_u)}{x_u} \qquad (Eq.7.21)$$

$$\varepsilon_{fu} = \frac{\varepsilon_{cu}\ (d_f - x_u)}{x_u} \qquad (Eq.7.22)$$

The stresses in the steel reinforcement and SIFCON parallel can be calculated using equations 7.23 and 7.24, respectively:

$$\sigma_{su} = E_s \varepsilon_{su} \qquad (Eq.7.23)$$

$$\sigma_{fu} = E_f \varepsilon_{fu} \qquad (Eq.7.24)$$

As shown in Figure 7.5 and using the force couple method to determine the neutral axis, x_u can be determined by:

$$C_{cu} = T_{su} + T_{fu} \qquad (Eq. 7.25)$$

Where C_{cu} is the compression force in concrete, T_{su} is the tension force in the steel reinforcement, and T_{fu} is the tension force in the composite.

$$0.85 f_c' b(0.85 x_u) = \sigma_{su} A_s + \sigma_{fu} A_f \qquad (Eq. 7.26)$$

It has been confirmed that after substituting the value of x_u in equation 7.22, the strain of SIFCON parallel will result in the ultimate strain capacity of SIFCON, as described previously in section 7.1.

To calculate the ultimate moment capacity, we sum the moment about C_{cu} as shown in equation 7.27:

$$M_u = \sigma_{su} A_s \left(d_s - \frac{0.85 x_u}{2} \right) + \sigma_{fu} A_f \left(d_f - \frac{0.85 x_u}{2} \right) \qquad (Eq. 7.27)$$

Where x_u is the depth of the rectangular compressive block from the fiber of maximum compressive strain, σ_{fu} is the ultimate strength of the fiber composite, σ_{su} is the ultimate strength of the steel reinforcement, and all others parameters are as defined previously.

In case where the system is not reinforced with steel, A_s should be replaced with zero

and equation 7.21 is not applicable.

The applied load can be obtained using the following equation:

$$P_u = M_u \frac{4}{L} \qquad (Eq. 7.28)$$

The ultimate curvature is found using the following equation:

$$\emptyset_u = \frac{\varepsilon_{cu}}{x_u} \qquad (Eq. 7.29)$$

Finally, the ultimate deflection can be obtained from the conjugate beam method:

$$\Delta_u = (\emptyset_u - \emptyset_{cr}) \frac{L}{2} \frac{h}{2} + \Delta_{cr} \qquad (Eq. 7.30)$$

Where $(\emptyset_u - \emptyset_{cr}) \frac{L}{2} \frac{h}{2}$ represents the deformation of the plastic hinge happening in the middle of the beam with a length of $\frac{h}{2}$ and Δ_{cr} represents the deformation at first crack as obtained from equation 7.4.

For FRP, FRC, & SIFCON Perpendicular:

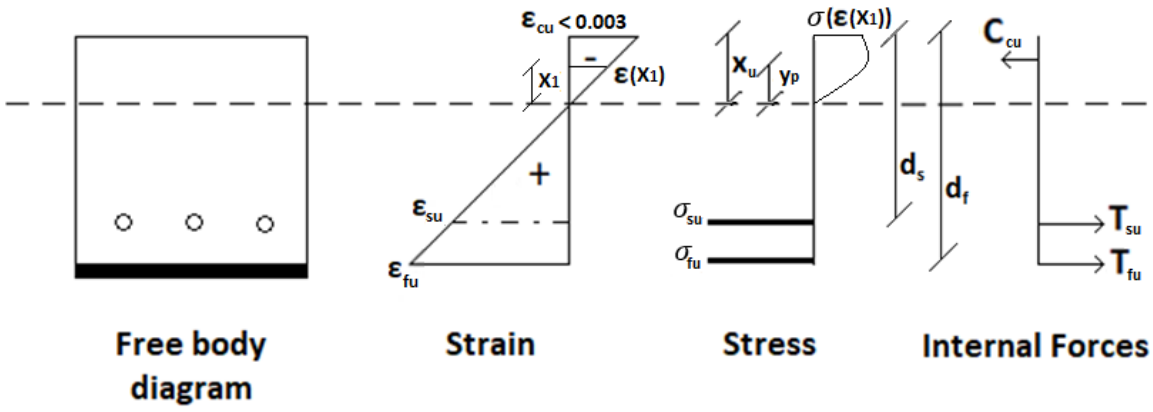

Figure 7. 6 - Bending relationships at ULS with steel reinforcement and retrofitted with FRP, FRC, or SIFCON perpendicular

Using similar triangles, equation 7.31 determines the strain of concrete as a function of x_1.

$$\varepsilon(x_1) = \frac{x_1 \varepsilon_{fu}}{(d_f - x_u)} \qquad (Eq. 7.31)$$

Where the strain at peak (ε_{fu}) varies based on the composite used:

- FRP: $\varepsilon_{fu} = \varepsilon_{fd}$ $(Eq. 7.32)$

  The strain in the fiber for FRP is the delamination strain as shown in literature review Eq. 5.5, as per ACI 440.2R-08.

- FRC:

  The peak strain (ε_{fu}) in FRC is as obtained by a study conducted by Lim, Paramasivam, and Lee (1987).

- SIFCON Perpendicular:

  The strain at ultimate conditions (ε_{fu}) is determined by a study conducted by Naaman and Homrich (1989).

The strain in SIFCON perpendicular is strain at ultimate capacity. SIFCON perpendicular peak strain.

Using similar triangles, equation 7.33 determines the strain of steel as a function of x_u.

$$\varepsilon_{su} = \frac{\varepsilon_{fu}\,(d_s - x_u)}{(d_f - x_u)} \qquad (Eq.\,7.33)$$

The compression stress of concrete is calculated using the equation of Todeschini et al. (1964).

$$\sigma(\varepsilon(x_1)) = \frac{2f_c'\left(\frac{\varepsilon(x_1)}{\varepsilon_0}\right)}{1 + \left(\frac{\varepsilon(x_1)}{\varepsilon_0}\right)^2} \qquad (Eq.\,7.34)$$

$$\text{Having} \quad \varepsilon_0 = 1.71\frac{f_c'}{E_c} \qquad (Eq.\,7.35)$$

Where $\varepsilon(x_1)$ represents the strain at a specific location x_1 in the concrete and ε_0 refers to a constant that represents the reference strain.

As shown in Figure 7.6 and using the force couple method to determine the neutral axis, x_u can be determined by equation 7.37:

$$C_{cu} = T_{su} + T_{fu} \qquad (Eq.\,7.36)$$

$$\int_0^{x_u} \frac{2f_c'\left(\frac{\varepsilon(x_1)}{\varepsilon_0}\right)}{1 + \left(\frac{\varepsilon(x_1)}{\varepsilon_0}\right)^2}\, dx_1 b = A_s E_s \varepsilon_{su} + A_f \sigma_{fu} \qquad (Eq.\,7.37)$$

Where σ_{fu} varies based on the composite used:

- FRP: $\sigma_{fu} = E_f e_{fd}$ $(Eq. 7.38)$

  The strain in the fiber for FRP is the delamination strain as shown in literature review Eq. 5.5, as per ACI 440.2R-08.

- FRC:

  The peak stress (σ_{fu}) in FRC is as obtained by a study conducted by Lim, Paramasivam, and Lee (1987).

- SIFCON Perpendicular:

  The stress at ultimate conditions (σ_{fu}) is determined by a study conducted by Naaman and Homrich (1989).

In order to determine the centroid of compression force of concrete (y_p), the following equation is used:

$$y_p = \frac{\int_0^x x_1 \frac{2f_c'\left(\frac{\varepsilon(x_1)}{\varepsilon_0}\right)}{1+\left(\frac{\varepsilon(x_1)}{\varepsilon_0}\right)^2} dx_1 b}{\int_0^x \frac{2f_c'\left(\frac{\varepsilon(x_1)}{\varepsilon_0}\right)}{1+\left(\frac{\varepsilon(x_1)}{\varepsilon_0}\right)^2} dx_1 b} \qquad (Eq. 7.39)$$

To calculate the ultimate moment capacity, we sum the moment about the resultant compression force of concrete, as shown in equation 7.40:

$$M_u = \sigma_{su} A_s \left((d_s - x_u) + y_p\right) + \sigma_{fu} A_f \left(\left(d_f - x_u\right) + y_p\right) \qquad (Eq. 7.40)$$

Where x_u is the depth of the rectangular compressive block from the fiber of maximum compressive strain, σ_{fu} is the ultimate strength of the fiber composite, σ_{su} is the ultimate strength of the steel reinforcement, and all others parameters are as defined previously.

In case where the system is not reinforced with steel, A_s should be replaced with zero and equation 7.33 is not applicable. The applied load can be obtained using the following equation:

$$P_u = M_u \frac{4}{L} \qquad (Eq. 7.41)$$

The ultimate curvature is found using the following equation:

$$\emptyset_u = \frac{\varepsilon_{fu}}{(d_f - x_u)} \qquad (Eq. 7.42)$$

Finally, the ultimate deflection can be obtained from the conjugate beam method:

For FRP & FRC: $\Delta_u = (\emptyset_u - \emptyset_y)\frac{L}{2}\frac{h}{2} + \Delta_y$ $(Eq. 7.43)$

For SIFCON perpendicular: $\Delta_u = (\emptyset_u - \emptyset_{cr})\frac{L}{2}\frac{h}{2} + \Delta_{cr}$ $(Eq. 7.44)$

Where $(\emptyset_u - \emptyset_y)\frac{L}{2}\frac{h}{2}$ and $(\emptyset_u - \emptyset_{cr})\frac{L}{2}\frac{h}{2}$ represents the deformation of the plastic hinge happening in the middle of the beam for either composite with a length of $\frac{h}{2}$. Δ_{cr} and Δ_y represent the deformation at first crack and yield as obtained from equation 7.4 and 7.20, respectively.

Rupture Phase of Composite for Sections with Steel Reinforcement

This phase is applicable to concrete sections with steel reinforcement and in the case where the composite ruptures:

For SIFCON parallel:

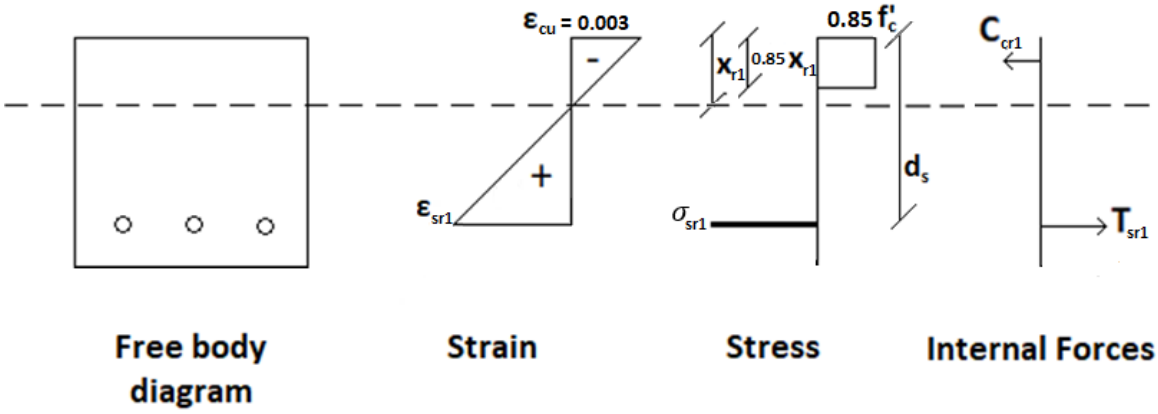

Figure 7. 7 - Bending relationships at rupture with steel reinforcement and retrofitted with SIFCON parallel composite

Wittney block is used since the strain in concrete (ε_{cu}) is 0.003.

Using similar triangles, equation 7.45 determines the strain as a function of x_{r1} in steel reinforcement.

$$\varepsilon_{sr1} = \frac{\varepsilon_{cu}\ (d_s - x_{r1})}{x_{r1}} \qquad (Eq.7.45)$$

The stress in the steel reinforcement can be calculated using equation 7.46:

$$\sigma_{sr1} = E_s \varepsilon_{sr1} \qquad (Eq.7.46)$$

As shown in Figure 7.7 and using the force couple method to determine the neutral

axis, x_{r1} can be determined by:

$$C_{cr1} = T_{sr1} \qquad (Eq. 7.47)$$

Where C_{cr1} is the compression force in concrete and T_{sr1} is the tension force in the steel reinforcement.

$$0.85 f_c' b(0.85 x_{r1}) = \sigma_{sr1} A_s \qquad (Eq. 7.48)$$

To calculate the rupture moment capacity, we sum the moment about C_{cr1} as shown in equation 7.49:

$$M_{r1} = \sigma_{sr1} A_s \left(d_s - \frac{0.85 x_{r1}}{2} \right) \qquad (Eq. 7.49)$$

Where σ_{sr1} is the rupture strength of the steel reinforcement, and all others parameters are as defined previously. The applied load can be obtained using the following equation:

$$P_{r1} = M_{r1} \frac{4}{L} \qquad (Eq. 7.50)$$

The rupture curvature is found using the following equation:

$$\emptyset_{r1} = \frac{\varepsilon_{cu}}{x_{r1}} \qquad (Eq. 7.51)$$

Finally, the rupture deflection can be obtained from the conjugate beam method:

$$\Delta_{r1} = (\emptyset_{r1} - \emptyset_u) \frac{L}{2} \frac{h}{2} + \Delta_u \qquad (Eq. 7.52)$$

Where $(\emptyset_{r1} - \emptyset_u) \frac{L}{2} \frac{h}{2}$ represents the deformation of the plastic hinge happening in the

middle of the beam with a length of $\frac{h}{2}$ and Δ_u represents the deformation at ultimate as obtained from equation 7.30.

For FRP, FRC, & SIFCON Perpendicular:

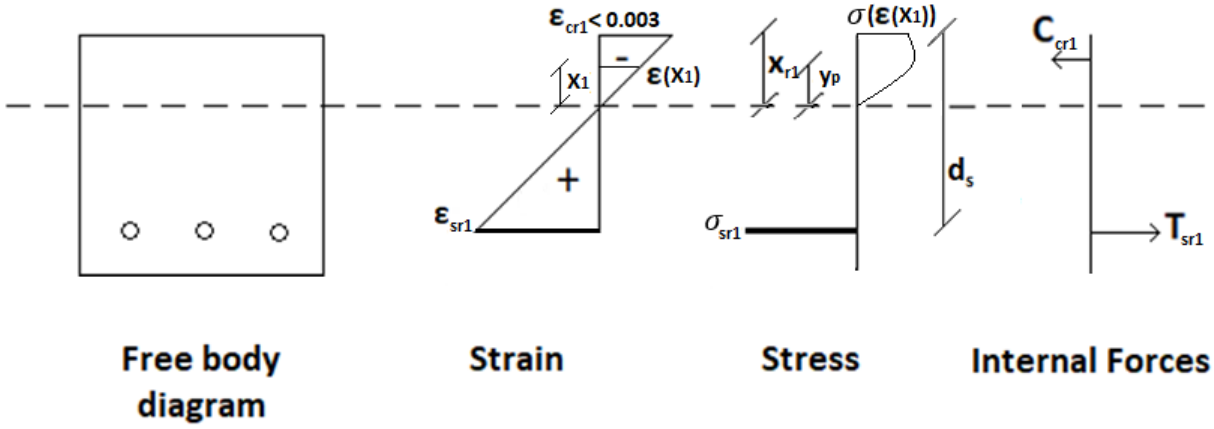

Figure 7. 8 - Bending relationships at rupture with steel reinforcement and retrofitted with FRP, FRC, or SIFCON perpendicular

The strain of concrete is the value obtained in the ultimate phase for each composite, as shown in the previous section.

Using similar triangles, equation 7.53 determines the strain of concrete as a function of x_1.

$$\varepsilon(x_1) = \frac{x_1 \varepsilon_{cr1}}{x_{r1}} \qquad (Eq.\ 7.53)$$

Using similar triangles, equation 7.54 determines the strain of steel as a function of x_{r1}.

$$\varepsilon_{sr1} = \frac{\varepsilon_{cr1}\,(d_s - x_{r1})}{x_{r1}} \qquad (Eq.\ 7.54)$$

Where ε_{cr1} represents the ultimate strain as obtained in the previous phase.

The compression stress of concrete is calculated using the following equation of

Todeschini et al. (1964).

$$\sigma(\varepsilon(x_1)) = \frac{2f_c'\left(\frac{\varepsilon(x_1)}{\varepsilon_0}\right)}{1+\left(\frac{\varepsilon(x_1)}{\varepsilon_0}\right)^2} \qquad (Eq.\,7.55)$$

$$\text{Having} \quad \varepsilon_0 = 1.71\frac{f_c'}{E_c} \qquad (Eq.\,7.56)$$

As shown in Figure 7.8 and using the force couple method to determine the neutral axis, x_{r1} can be determined by equation 7.58:

$$C_{cr1} = T_{sr1} \qquad (Eq.\,7.57)$$

$$\int_0^{x_{r1}} \frac{2f_c'\left(\frac{\varepsilon(x_1)}{\varepsilon_0}\right)}{1+\left(\frac{\varepsilon(x_1)}{\varepsilon_0}\right)^2}\, dx_1 b = A_s E_s \varepsilon_{sr1} \qquad (Eq.\,7.58)$$

To calculate the rupture moment capacity, we sum the moment about the resultant compression force of concrete, as shown in equation 7.59:

$$M_{r1} = A_s E_s \varepsilon_{sr1}\left((d_s - x_{r1}) + y_p\right) \qquad (Eq.\,7.59)$$

Where y_p is obtained as defined previously in equation 7.39, x_{r1} is the depth of the rectangular compressive block from the fiber of maximum compressive strain, σ_{sr1} is the strength of the steel reinforcement, and all others parameters are as defined previously.

The applied load is calculated using the same load equation of Eq.7.50.

The rupture curvature is found using the following equation:

$$\emptyset_{r1} = \frac{\varepsilon_{sr1}}{(d_s - x_{r1})} \qquad (Eq.7.60)$$

Finally, the rupture deflection can be obtained from the conjugate beam method:

$$\Delta_{r1} = (\emptyset_{r1} - \emptyset_u)\frac{L}{2}\frac{h}{2} + \Delta_u \qquad (Eq.7.61)$$

Where $(\emptyset_{r1} - \emptyset_u)\frac{L}{2}\frac{h}{2}$ represents the deformation of the plastic hinge happening in the middle of the beam with a length of $\frac{h}{2}$ and Δ_u represents the deformation at ultimate as obtained from equations 7.43 and 7.44.

Failure of Section

For sections without steel reinforcement in the specimen:

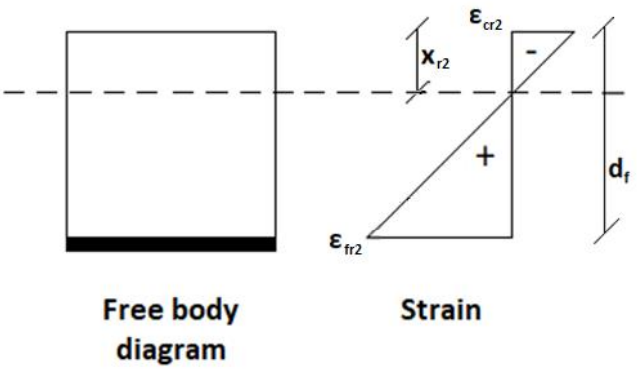

Figure 7. 9 - Bending relationships at rupture without steel reinforcement and retrofitted a composite

Using similar triangles, equation 7.62 determines x_{r2} using the strain in the concrete ε_{cr2} as obtained previously from the previous phase and the rupture strain ε_{fr2} depends on the composite used:

- FRP: as obtained from the manufactural data sheet of Tyfo.
- FRC: as obtained by Lim, Paramasivam, and Lee (1987).
- SIFCON: as determined by Naaman and Homrich (1989).

$$\frac{\varepsilon_{fr2}}{(d_f - x_{r2})} = \frac{\varepsilon_{cr2}}{x_{r2}} \qquad (Eq. 7.62)$$

Rupture moment capacity:

$$M_{r2} = 0 \qquad (Eq. 7.63)$$

Applied load:

$$P_{r2} = 0 \qquad (Eq. 7.64)$$

The rupture curvature is found using the following equation:

$$\emptyset_{r2} = \frac{\varepsilon_{cr2}}{x_{r2}} \qquad (Eq.7.65)$$

Finally, the rupture deflection can be obtained from the conjugate beam method:

$$\Delta_{r2} = (\emptyset_{r2} - \emptyset_u)\frac{L}{2}\frac{h}{2} + \Delta_u \qquad (Eq.7.66)$$

<u>In case the steel reinforcement ruptures in specimen for sections with steel reinforcement:</u>

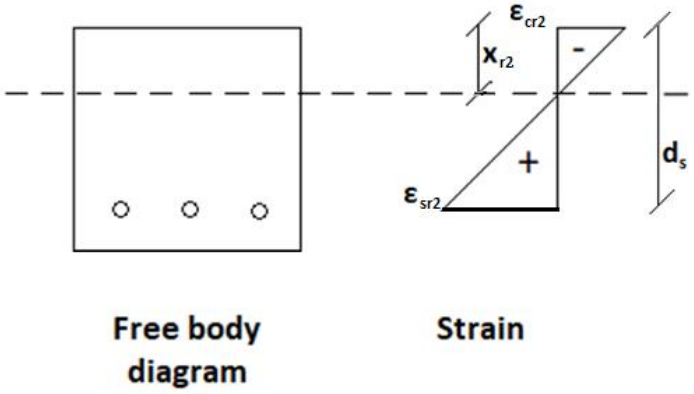

Figure 7. 10 - Bending relationships at rupture of steel reinforcement

Using similar triangles, equation 7.67 determines x_{r2} using the strain in the concrete and the strain in the steel reinforcement that are ε_{cr2} and rupture strain of steel from the manufactural data sheet of Tyfo, respectively.

$$\frac{\varepsilon_{sr2}}{(d_s - x_{r2})} = \frac{\varepsilon_{cr2}}{x_{r2}} \qquad (Eq.7.67)$$

Rupture moment capacity:

$$M_{r2} = 0 \qquad (Eq. 7.68)$$

Applied load:

$$P_{r2} = 0 \qquad (Eq. 7.69)$$

The rupture curvature is found using the following equation:

$$\emptyset_{r2} = \frac{\varepsilon_{cr2}}{x_{r2}} \qquad (Eq. 7.70)$$

Finally, the rupture deflection can be obtained from the conjugate beam method:

$$\Delta_{r2} = (\emptyset_{r2} - \emptyset_{r1}) \frac{L}{2} \frac{h}{2} + \Delta_{r1} \qquad (Eq. 7.71)$$

All variables in the above equations are defined in section 10 (List of Notations).

Load-Deflection and Moment-Curvature Response

The load-deflection graph shown in Figure 7.1 can be obtained using the following equations where all parameters are obtained in the model response section.

$$P = \Delta \frac{P_{cr}}{\Delta_{cr}} \ for \ \Delta \ \leq \ \Delta_{cr} \qquad (7.72)$$

$$P = P_{cr} + \left(P_y - \ P_{cr}\ \right) \frac{(\Delta \ - \ \Delta_{cr})}{\left(\Delta_y \ - \ \Delta_{cr}\right)} \quad for \ \Delta_{cr} \ < \ \Delta \ \leq \Delta_y \qquad (7.73)$$

$$P = P_y + \left(P_u - \ P_y\ \right) \frac{\left(\Delta \ - \ \Delta_y\right)}{\left(\Delta_u \ - \ \Delta_y\right)} \quad for \ \Delta_y < \ \Delta \ \leq \ \Delta_u \qquad (7.74)$$

$$P = P_u + (P_{r1} - \ P_u\ ) \frac{(\Delta \ - \ \Delta_u)}{(\Delta_{r1} \ - \ \Delta_u)} \quad for \ \Delta_u < \ \Delta \ \leq \ \Delta_{r1} \qquad (7.75)$$

$$P = P_{r1} + (P_{r2} - \ P_{r1}\ ) \frac{(\Delta \ - \ \Delta_{r1})}{(\Delta_{r2} \ - \ \Delta_{r1})} \quad for \ \Delta > \ \Delta_{r1} \qquad (7.76)$$

For sections without steel reinforcement, equation 7.76 is not applicable and P_{r1} is replaced with P_{r2} in equation 7.75.

The Moment-Curvature graph shown in Figure 7.2 can be obtained using the following equations where all parameters are obtained in the model response section.

$$M = \emptyset \frac{M_{cr}}{\emptyset_{cr}} \ for \ \emptyset \ \leq \ \emptyset_{cr} \qquad (7.78)$$

$$M = M_{cr} + \left(M_y - M_{cr}\right) \frac{(\emptyset - \emptyset_{cr})}{(\emptyset_y - \emptyset_{cr})} \quad for\ \emptyset_{cr} < \emptyset \leq \emptyset_y \qquad (7.79)$$

$$M = M_y + \left(M_u - M_y\right) \frac{(\emptyset - \emptyset_y)}{(\emptyset_u - \emptyset_y)} \quad for\ \emptyset_y < \emptyset \leq \emptyset_u \qquad (7.80)$$

$$M = M_u + (M_{r1} - M_u) \frac{(\emptyset - \emptyset_u)}{(\emptyset_{r1} - \emptyset_u)} \quad for\ \emptyset_u < \emptyset \leq \emptyset_{r1} \qquad (7.81)$$

$$M = M_{r1} + (M_{r2} - M_{r1}) \frac{(\emptyset - \emptyset_{r1})}{(\emptyset_{r2} - \emptyset_{r1})} \quad for\ \emptyset > \emptyset_{r1} \qquad (7.82)$$

For sections without steel reinforcement, equation 7.82 is not applicable and M_{r1} is replaced with M_{r2} in equation 7.81.

The translational and rotational stiffness are

$$K_y = \frac{P_y - P_{cr}}{\Delta_y - \Delta_{cr}} \qquad (7.83)$$

$$E_y I_y = \frac{M_y - M_{cr}}{\emptyset_y - \emptyset_{cr}} \qquad (7.84)$$

8. COMPARISON OF EXPERIMENTAL AND ANALYTICAL DATA

The graphs in Figures 8.1 to 8.4 and Tables 8.1 and 8.2 present a comparison between the experimental and analytical results of polymers and cementitious composites with and without steel.

Among the polymer composites tested for retrofitting concrete beams, Glass SEH 51 exhibited the greatest difference of 185% between theoretical and experimental values for the critical deflection. Carbon 11 UP demonstrated largest difference of around 14% in critical load capacity. Glass SEH 51 also showed the largest discrepancy for delta yield and yield load with 55.5% and 49%, respectively. The maximum difference in delta ultimate was observed in Carbon SCH 41 with a value of 122%. Moreover, Glass SEH 51 showed the greatest difference in the ultimate load capacity of around 22%. Carbon 11 UP showed the largest difference in the deflection rupture with a value of 3%, while Carbon SCH 41 had the greatest difference in rupture load between theoretical and experimental values, with a difference of approximately 35%. Additionally, Carbon 11 UP exhibited the greatest difference in delta rupture 2 among all polymer composites, with a value of 59%.

Among the cementitious composites tested for retrofitting concrete beams, SIFCON parallel and perpendicular showed the highest discrepancy of around 31% between theoretical and experimental critical deflection. FRC established the largest difference of around 22% in critical load capacity. In addition, FRC exhibited the greatest difference for delta yield and yield load with 8.3% and 6.6%, respectively. The maximum difference in delta ultimate was detected in SIFCON perpendicular with a

value of 45%. Furthermore, SIFCON parallel showed the greatest difference in the ultimate load capacity among cementitious composites of around 49.5%. SIFCON perpendicular showed the major difference in delta rupture with a negligible value of 1.4%, while FRC had the largest difference in rupture load between theoretical and experimental values, with a difference of approximately 53%. Moreover, FRC showed the greatest difference in the deflection rupture 2 among all polymer composites, with a value of 59%.

The observed discrepancies could be explained by a variety of causes. Assumptions made during the theoretical study, such as the failure criteria applied or the modeling of the material behavior, may have been neglected as per the assumptions defined previously. The quality of the materials used during the experimental testing, as well as changes in the testing processes and settings, could be another reason for the variances. The nature and severity of the damage sustained during loading, as well as the bonding properties between the polymer composites and the concrete specimen, may potentially have impacted the results. The observed discrepancies between theoretical and experimental results may also be the result of other variables, such as human error or environmental conditions.

It is possible that the complex behavior of the materials under various loading circumstances was not properly taken into account by the theoretical models used to forecast the behavior of the retrofitted beams. There could have been model assumptions that didn't accurately reflect how the materials behaved in the experiments. Additionally, the polymer composites' performance in the studies could have varied from what was anticipated theoretically because of variability in the manufacturing or installation process.

Variations in the testing conditions itself, such as the rate of loading, the temperature,

and the humidity, may have had an effect on the behavior of the materials in ways that weren't predicted by the theoretical models.

Improper laying of steel fibers in the SIFCON mix may have led to deficiencies in the structural integrity and performance of the composite. Inadequate dispersion of the fibers within the mix is one of the most common errors, which can result in areas of the concrete with low fiber content and reduced strength and ductility. Moreover, improper alignment or orientation of the fibers may prevent them from successfully resisting the tensile stresses that arise during loading, which could cause early cracking and collapse of the concrete.

Another error that could also occur during laying steel fibers is poor mixing, which can cause the fibers to clump together and cause voids or weak regions in the composite. This can significantly reduce the load capacity of the composite and result in premature failure. Overall, most of the experimental data for composites showed close correlation with theoretical values.

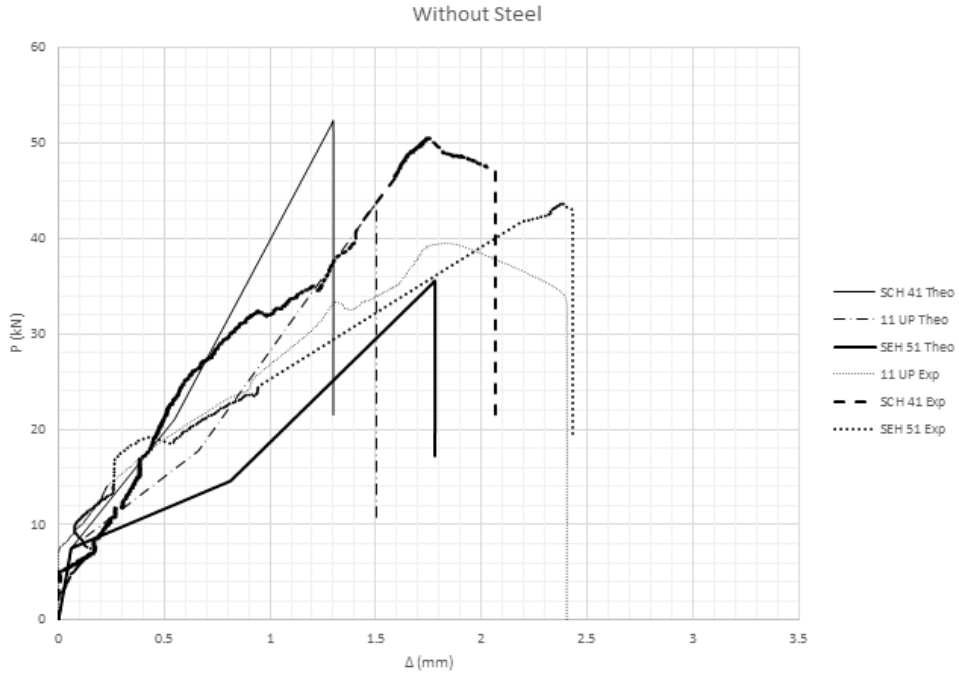

Figure 8. 1 - Polymers without steel theoretical and experimental comparison

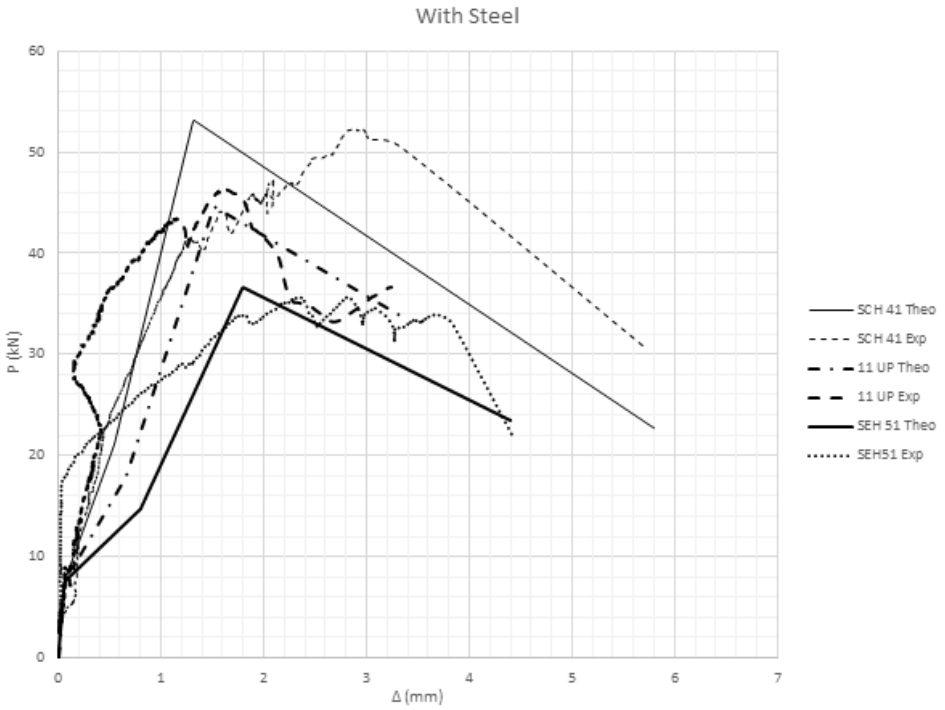

Figure 8. 2 - Polymers with steel theoretical and experimental comparison

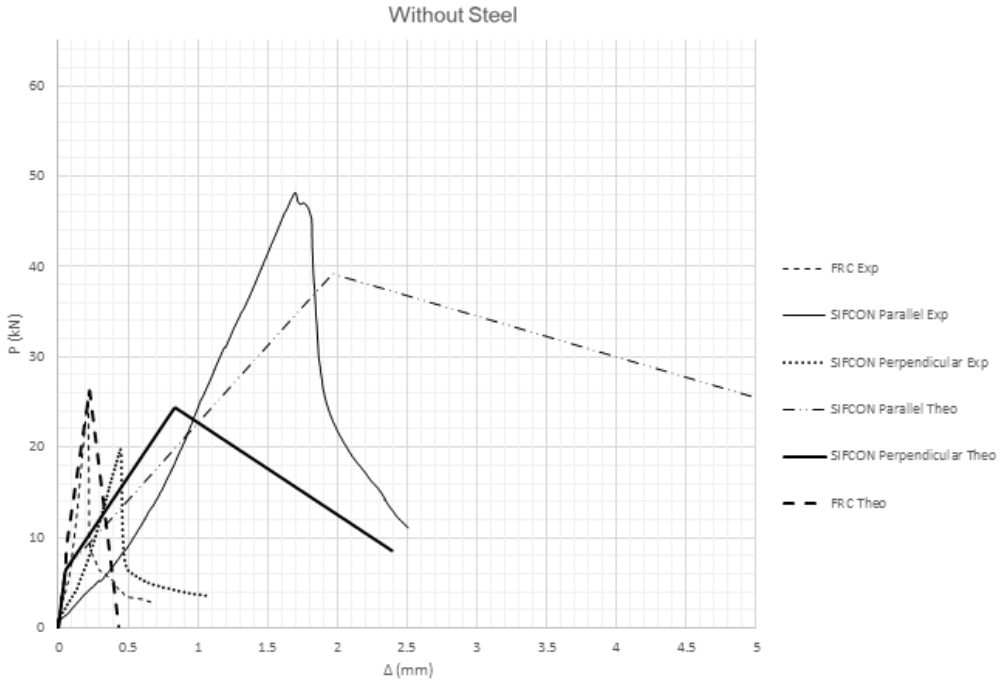

Figure 8. 3 - Cementitious composites without steel theoretical and experimental comparison

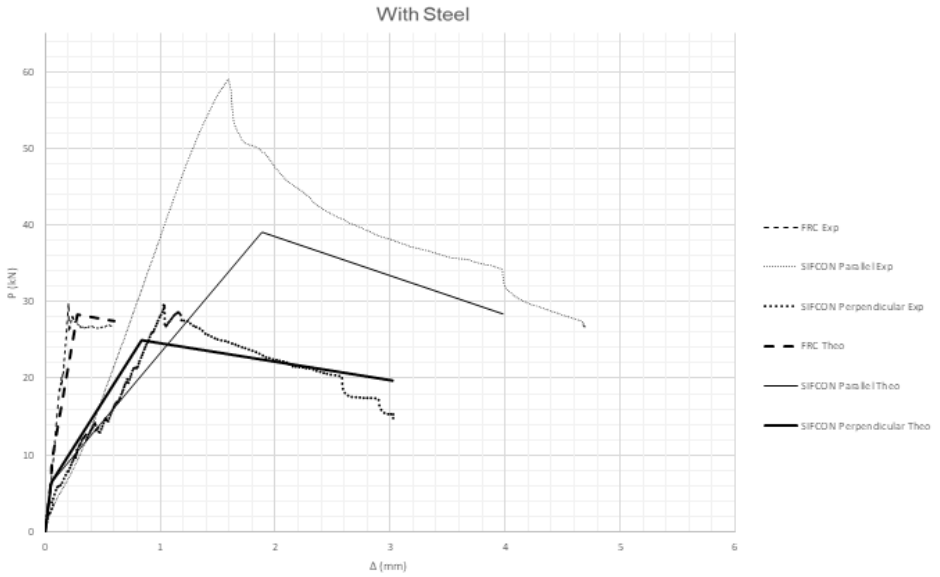

Figure 8. 4 - Cementitious composites with steel theoretical and experimental comparison

Table 8. 1 - Theoretical and experimental results of polymers and cementitious composites without steel reinforcement

		Without Steel																
		Δcr	Pcr	Δy	Py	Δ_U	P_U	Δ_{R1}	P_{R1}	Δ_{R2}	P_{R2}	μ	Stiffness Ky	Ey	Stiffness Kc	Ec	T	TI
		mm	kN	mm	kN	mm	kN	mm	kN	mm	kN		kN/mm	kN/mm2	kN/mm	kN/mm2	kN-mm	
Regular Conc	Exp	0.10	5.83	0.29	8.19	0.42	9.04	-	-	0.42	0.00	1.45	12.50	1.88	57.73	8.70	2.70	1.00
GLASS SEH - 51	Exp	0.17	7.16	0.55	18.61	2.39	43.54	-	-	2.43	0.00	4.43	30.27	31.71	41.89	6.31	44.56	16.48
	Theo	0.06	7.53	0.81	14.58	1.79	35.70	-	-	1.79	0.00	2.20	9.36	9.80	125.57	18.92	33.04	12.22
CARBON 11-UP	Exp	0.07	8.19	0.57	20.14	1.75	39.30	-	-	2.40	0.00	4.21	24.00	16.82	113.69	17.13	42.27	15.63
	Theo	0.06	7.53	0.66	17.72	1.51	43.89	-	-	1.51	0.00	2.28	16.94	11.87	125.57	18.92	33.84	12.51
CARBON SCH - 41	Exp	0.17	8.00	0.51	21.35	1.76	50.33	-	-	2.07	0.00	4.08	39.26	19.25	48.19	7.26	50.49	18.67
	Theo	0.06	7.53	0.55	21.03	1.31	52.70	-	-	1.31	0.00	2.39	27.59	13.53	125.57	18.92	35.22	13.02
FRC	Exp	0.05	4.97	0.06	8.45	0.22	25.54	-	-	0.69	2.80	11.19	348.00	27.47	95.58	14.40	3.70	1.37
	Theo	0.05	6.39	0.06	9.05	0.23	26.27	-	-	0.44	0.00	7.42	332.75	26.27	125.25	18.88	3.17	1.17
SIFCON Parallel	Exp	0.07	6.19	-	-	1.78	47.67	-	-	7.61	1.20	113.58	23.45	2.27	92.36	13.92	40.54	14.99
	Theo	0.05	6.39	-	-	1.97	39.23	-	-	7.50	0.00	147.06	18.21	1.76	125.25	18.88	43.91	16.24
SIFCON Perpendicular	Exp	0.07	5.90	-	-	0.46	19.51	-	-	2.70	3.57	40.30	43.20	3.84	88.10	13.28	5.21	1.93
	Theo	0.05	6.39	-	-	0.84	24.42	-	-	3.23	0.00	63.31	23.40	2.08	125.25	18.88	12.24	4.53

Table 8. 2 - Theoretical and experimental results of polymers and cementitious composites with steel reinforcement

		With Steel																
		Δcr	Pcr	Δy	Py	Δ_U	P_U	Δ_{R1}	P_{R1}	Δ_{R2}	P_{R2}	μ	Stiffness Ky	Ey	Stiffness Kc	Ec	T	TI
		mm	kN	mm	kN	mm	kN	mm	kN	mm	kN		kN/mm	kN/mm2	kN/mm	kN/mm2	kN-mm	
Regular Conc	Exp	0.09	1.33	0.34	5.19	0.51	7.53	-	-	0.82	5.11	2.40	15.55	309.09	14.34	2.16	5.13	1.00
GLASS SEH - 51	Exp	0.07	8.56	0.36	21.95	2.84	35.54	4.43	21.77	15.31	0.00	12.43	46.19	47.15	129.67	19.54	121.55	23.70
	Theo	0.06	7.53	0.80	14.72	1.80	36.65	4.40	23.47	15.47	0.00	5.50	9.71	9.91	125.57	18.92	112.32	21.90
CARBON 11-UP	Exp	0.15	8.61	0.41	22.05	1.66	46.19	3.24	36.65	15.10	0.00	7.86	50.34	34.72	59.34	8.94	112.72	21.98
	Theo	0.06	7.53	0.65	17.81	1.51	44.58	3.34	33.72	15.47	0.00	5.11	17.30	11.93	125.57	18.92	106.08	20.68
CARBON SCH - 41	Exp	0.14	7.21	0.44	22.93	2.92	52.19	5.73	30.61	15.30	0.00	12.98	52.75	25.62	50.42	7.60	214.27	41.78
	Theo	0.06	7.53	0.55	21.09	1.31	53.19	5.80	22.70	15.47	0.00	10.64	27.95	13.57	125.57	18.92	205.96	40.16
FRC	Exp	0.05	6.36	0.07	9.70	0.20	29.05	8.10	3.51	15.12	0.00	124.62	257.31	20.29	122.23	18.42	5.31	1.03
	Theo	0.05	6.39	0.06	9.23	0.28	28.41	8.09	7.49	15.47	0.00	134.90	315.56	24.89	125.25	18.88	4.35	0.85
SIFCON Parallel	Exp	0.06	7.61	-	-	1.60	58.42	8.05	7.02	15.10	0.00	129.84	36.20	3.55	122.81	18.51	262.04	51.09
	Theo	0.05	6.39	-	-	1.89	39.08	8.09	7.49	15.46	0.00	158.67	19.20	1.88	125.25	18.88	186.36	36.33
SIFCON Perpendicular	Exp	0.07	5.74	-	-	1.04	28.80	7.98	3.87	15.20	0.00	120.91	30.81	2.81	86.89	13.10	130.37	25.42
	Theo	0.05	6.39	-	-	0.84	24.99	8.09	7.49	15.46	0.00	158.67	24.33	2.22	125.25	18.88	130.28	25.40

9. CONCLUSION & RECOMMENDATION

The integration of composite materials in particular using cementitious in lieu of polymer composites has resulted in a more sustainable and resilient long-term structure. Hence, investigating the flexural behavior of concrete beams retrofitted with different composite materials has been in demand. FRP composites have been used extensively as reinforcement in the construction industry for reinforced structures as a substitute for conventional steel due to its lightweight, high tensile strength, and non-corrosive properties. New developed cementitious composite materials require further investigation for construction applications. The focus of this research is to develop a comparative study of the flexural behaviors of reinforced and non-reinforced concrete beams retrofitted with FRC and SIFCON compared to GFRP and CFRP. The research focuses on the experimental and analytical investigation of reinforced and unreinforced beams retrofitted with different composites and develops models for the load-deflection and moment-curvature response.

The following can be concluded from the research study herein:

- Steel reinforcement improves the ductile behavior in flexure with a post-peak softening response after reaching peak leading to tougher material. The presence of steel reinforcement will improve the ductile behavior of the beams for the different composite retrofits however the improvement is more evident for SIFCON with fibers aligned in the tensile direction due to its highest strain at peak. Steel reinforcement in retrofitted beams slightly improved the peak loads, but predominantly the ductility of the system (independent of the type of

composite).

- Concrete beams retrofitted with Carbon SCH 41, SCH 11 UP, and Glass SEH 51 resulted in the highest peak loads (high toughness) with a relatively low rupture strains with low ductility compared to the other composites. It also exhibited high elastic moduli resulting in higher stiffness. Such polymer composite retrofits are recommended for gravity load resistance and not for seismic loading. In order to resist seismic loads, materials require to be more flexible with higher ductility ratios and not necessarily higher peak loads.

- Beams retrofitted with FRP composites resulted in a brittle failure when no steel reinforcement was introduced. The steel reinforcement improved the ductility of the system yet was not as effective as when used in beams retrofitted with cementitious composites, in particular for SIFCON with fibers parallel to the tension direction. This is due to the brittle nature of FRP. Thus FRP retrofits are not suitable for seismic load resistance.

- Beams retrofitted with FRC composites exhibited low peak flexural strength values. The rupture strains and toughness are the lowest among all other composites. Due to the random orientation of the fibers, the ductility of the system is low. The behavior of the composite showed a single crack pattern in the middle of the beam and then a sudden failure resulted. On the other hand, it resulted in the highest stiffness values because of the stones present in the FRC mix. Thus this retrofit is not recommended as a retrofit option.

- SIFCON Parallel without steel reinforcement has the highest rupture strains and ductility ratio. In addition, it has the lowest stiffness and comparatively a high peak load and toughness. The orientation of the fibers lead to a multiple cracking mechanism that will enhance the softening behavior beyond peak. The multiple cracking mechanism improve ductility. Permeability due to the micro silica sand extends the rupture strains far beyond other composites. The high load capacity is due to the presence of fibers aligned in the tensile direction which adds to the presence of steel reinforcement and the fibers are at the same time ductile. Hence, SIFCON Parallel is highly recommended for earthquake events due to its flexibility, ductility, and high load capacity.

- SIFCON Perpendicular without steel reinforcement has the lowest peak strength values between all the non-steel reinforced composites and a significantly low toughness ability. Moreover, it has a low stiffness and ductility ratio higher than that of FRC composites with a considerably high strain rupture compared to FRP composites. The low stiffness is due to the large percentage of fiber volume fraction present that have a low stiffness. However, lack of ductility is due to the direction of the fibers that will not enhance the tensile behavior of the beam in flexure. Hence, it is not suitable for retrofit applications.

- Presented theoretical models show a good correlation with the experimental data. However, it should be noted that errors were found due to experimental variations.

In conclusion, retrofitted structures exhibiting high peak strengths with low rupture strains are suitable for resisting gravity loads and not necessarily seismic loading, such as in FRP retrofits. Although the steel reinforcement improves the ductility yet it is not as comparable as to cementitious composites with high volume fiber fraction aligned with the load direction. Retrofitted structures experiencing high peak loads with high rupture strains perform well under gravity and seismic loads, such as in SIFCON retrofits. A large stiffness is not suitable for earthquakes, for the material is required to be flexible during seismic activities. Random orientation of fibers as in FRC as well as fibers aligned perpendicular to the loading direction are not recommended for retrofits due to their low peak strengths and rupture strains even in the presence of steel reinforcement.

In order to reduce potential sources of error and improve the accuracy of the results, a wider range of factors should be considered, failure criteria should be improved, material behavior should be accurately modeled, high-quality materials should be used, standardized testing procedures should be implemented, and steel fibers should be applied carefully. These suggestions can help future research increase the accuracy of its findings.

Each retrofit method has its specific advantage in resisting a given load. Every material is suitable for a specific application, load condition, and installation feasibility. Regarding the ease of installation practicability, FRP is easily installed onsite, but may not be applicable in some areas which require infill. In addition, SIFCON has several restrictions for application on site and has a higher cost with respect to FRP, knowing that it demands intensive labor and contains relatively expensive steel. In addition, the pre-placement of the fibers is a challenge and requires extensive quality control.

The Use of Cementitious composites as retrofit options does not necessarily eliminate

the need for the use of FRP. Each of these two advanced standard retrofit techniques has a specific application for which it is best suited. Hence, the best design solution might be achieved if both can be used complementarily. Cementitious composites might be better suited for three-dimensional applications such zones of reinforcing bars anchorages or of beam-column joints. This is under investigation using 3D applications in the construction industry.

10. LIST OF NOTATIONS

The following symbols are used in this report:

A_s	Area of steel reinforcement
A_f	Area of composite fiber
b	Specimen width
C_{ccr}	Compression force of concrete at first crack
C_{cy}	Compression force of concrete at yield
C_{cu}	Compression force of concrete at ultimate
C_{cr1}	Compression force of concrete at composite rupture of specimen with steel reinforcement
D	Diameter of reinforcement rebar
d_s	Distance from steel reinforcement centroid to extreme compression fiber
d_f	Distance from composite centroid to extreme compression fiber
E_c	Modulus of elasticity of concrete
E_f	Modulus of elasticity of Fiber
E_s	Modulus of elasticity of steel
E_y	Modulus of elasticity of the system at yield
E'_y	Modulus of elasticity of SIFCON
e_{fd}	Delamination strain
ε_{ccr}	Strain of concrete at first crack
ε_{cy}	Strain of concrete at yield
ε_{cu}	Strain of concrete at ultimate

ε_{cr1}	Strain of concrete at composite rupture of specimen with steel reinforcement
ε_{cr2}	Strain of concrete at system failure
ε_{sy}	Strain of steel at yield
ε_{su}	Strain of steel at ultimate
ε_{sr1}	Strain of steel at composite rupture of specimen with steel reinforcement
ε_{sr2}	Strain of steel at system failure
ε_{fy}	Strain of composite at yield
ε_{fu}	Strain of composite at ultimate
ε_{fr2}	Strain of composite at system failure
$\varepsilon(x_1)$	Strain at distance x_1 in the concrete
ε_0	Constant strain reference
f'$_c$	Ultimate strength of concrete
h	Specimen thickness
I_c	Gross moment of inertia
I_y	Cracked moment of inertia
I'$_y$	Cracked moment of inertia of SIFCON
K_c	Stiffness of concrete
K_y	Stiffness of system at yield
K'$_y$	Stiffness of SIFCON
L	Beam specimen length
m	Number of polymer sheet layers
M_{cr}	Moment at first crack
M_y	Moment at yield

M_u	Moment at ultimate
M_{r1}	Moment at composite rupture of specimen with steel reinforcement
M_{r2}	Moment at system failure
$M_{r2\ No\ Steel}$	Moment at composite rupture of specimen without steel reinforcement
P_{cr}	Load at first crack
P_y	Load at yield
P_u	Load at ultimate
P_{r1}	Load at composite rupture of specimen with steel reinforcement
P_{r2}	Load at system failure
$P_{r2\ No\ Steel}$	Load at composite rupture of specimen without steel reinforcement
σ_{ccr}	Stress of concrete at first crack
σ_{cy}	Stress of concrete at yield
σ_{cu}	Stress of concrete at ultimate
σ_{cr1}	Stress of concrete at composite rupture of specimen with steel reinforcement
σ_{cr2}	Stress of concrete at system failure
σ_r	Modulus of rupture of concrete
σ_{sy}	Stress of steel at yield
σ_{su}	Stress of steel at ultimate
σ_{sr1}	Stress of steel at composite rupture of specimen with steel reinforcement
σ_{fy}	Stress of composite at yield

σ_{fu}	Stress of composite at ultimate
σ_{fr2}	Stress of composite at system failure
t_f	Thickness of fiber
T	Toughness of the system
TI	Toughness index
T_{ccr}	Tension force of concrete at first crack
T_{sy}	Tension force of steel at yield
T_{su}	Tension force of steel at ultimate
T_{sr1}	Tension force of steel at composite rupture of specimen with steel reinforcement
T_{fy}	Tension force of composite at yield
T_{fu}	Tension force of composite at ultimate
μ	Ductility ratio
$V_{specimen}$	Volume of specimen
x_y	Depth of neutral axis at yield
x_u	Depth of neutral axis at ultimate
x_{r1}	Depth of neutral axis at composite rupture of specimen with steel reinforcement
x_{r2}	Depth of neutral axis at system failure
y_p	Distance from neutral axis to centroid of compression force of concrete
Δ_{cr}	Deformation at first crack
Δ_y	Deformation at yield
Δ_u	Deformation at ultimate
Δ_{r1}	Deformation at composite rupture of specimen with steel

	reinforcement
$\Delta_{r2\ No\ Steel}$	Deformation at composite rupture of specimen without steel reinforcement
Δ_{r2}	Deformation at system failure
ϕ_{cr}	Curvature at first crack
ϕ_{y}	Curvature at yield
ϕ_{u}	Curvature at ultimate
ϕ_{r1}	Curvature at composite rupture of specimen with steel reinforcement
$\phi_{r2\ No\ Steel}$	Curvature at composite rupture of specimen without steel reinforcement
ϕ_{r2}	Curvature at system failure

APPENDIX I: EXPERIMENTAL RESULTS - GRAPHICAL AND TABULAR RESULTS

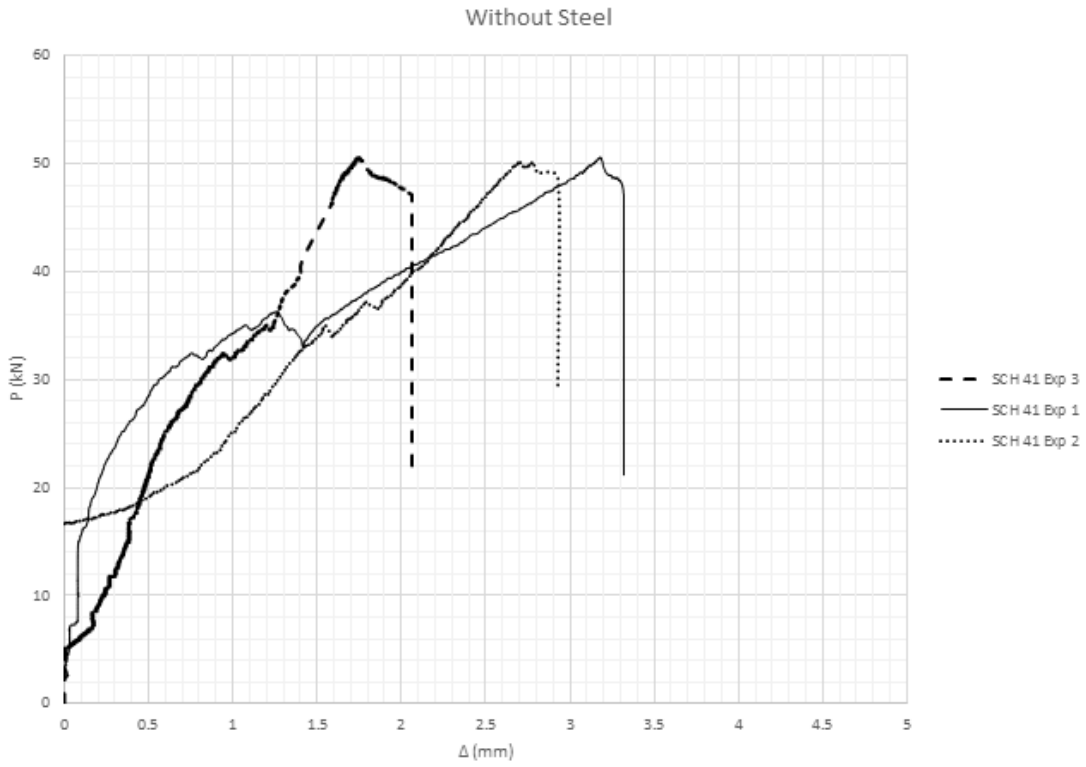

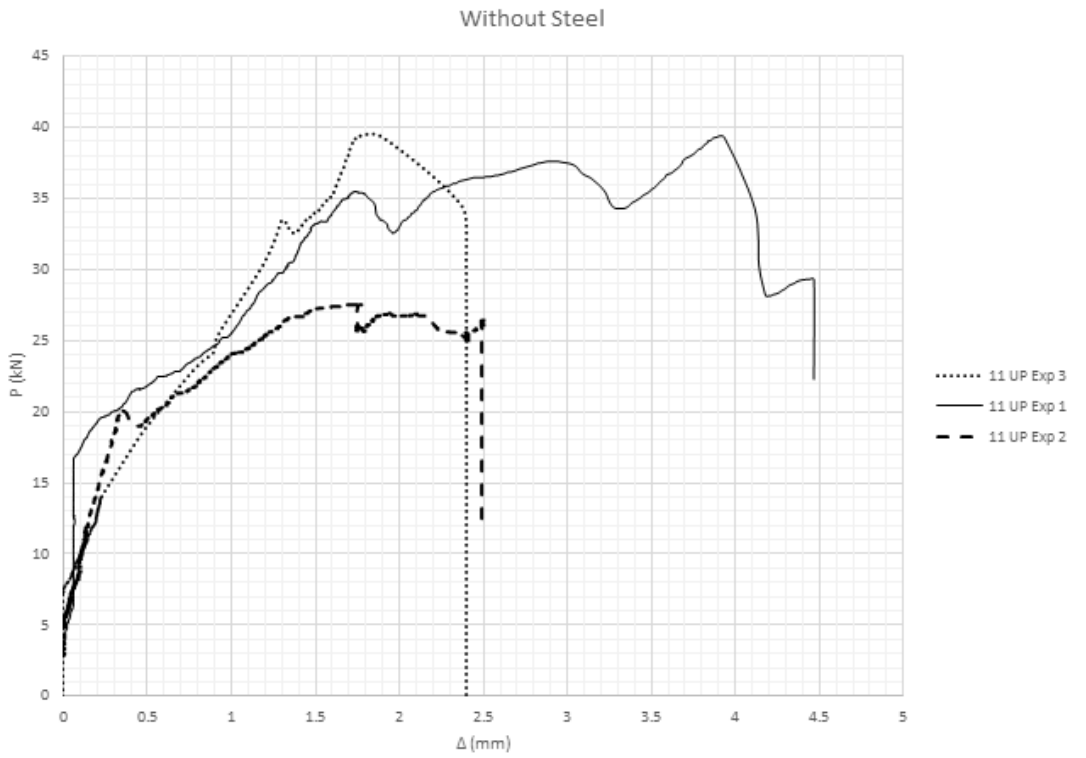

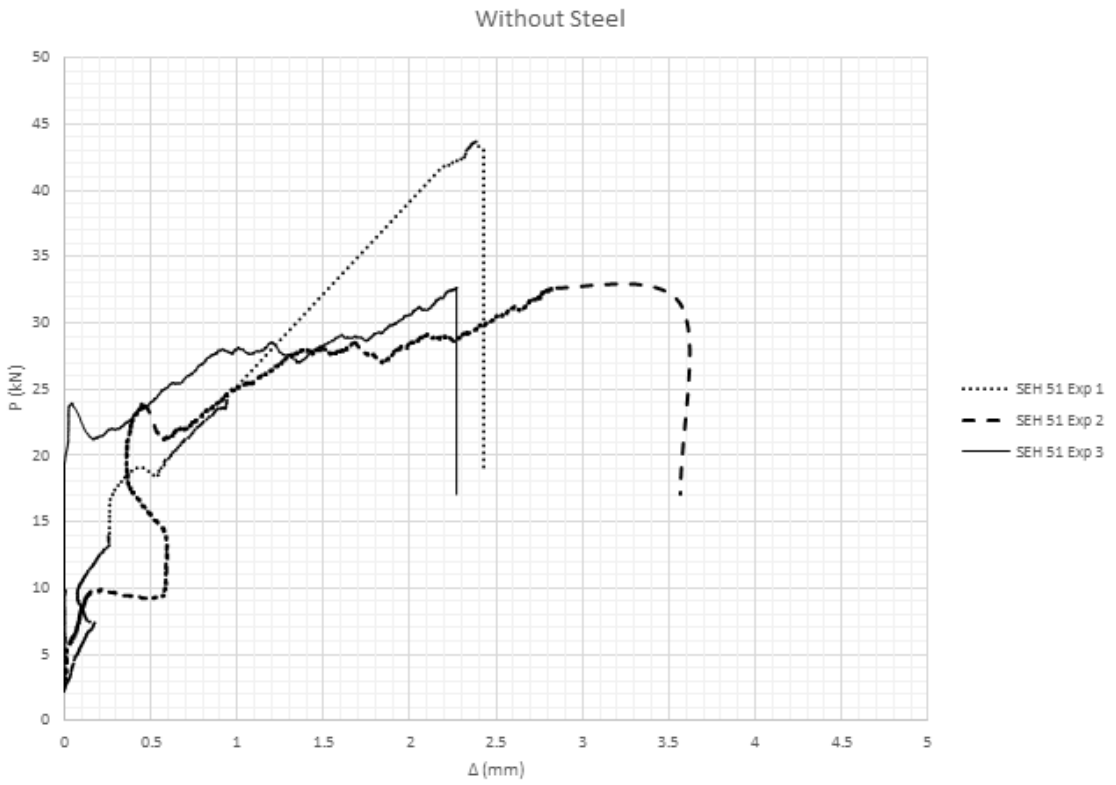
Without Steel
P (kN)
Δ (mm)
SEH 51 Exp 1
SEH 51 Exp 2
SEH 51 Exp 3

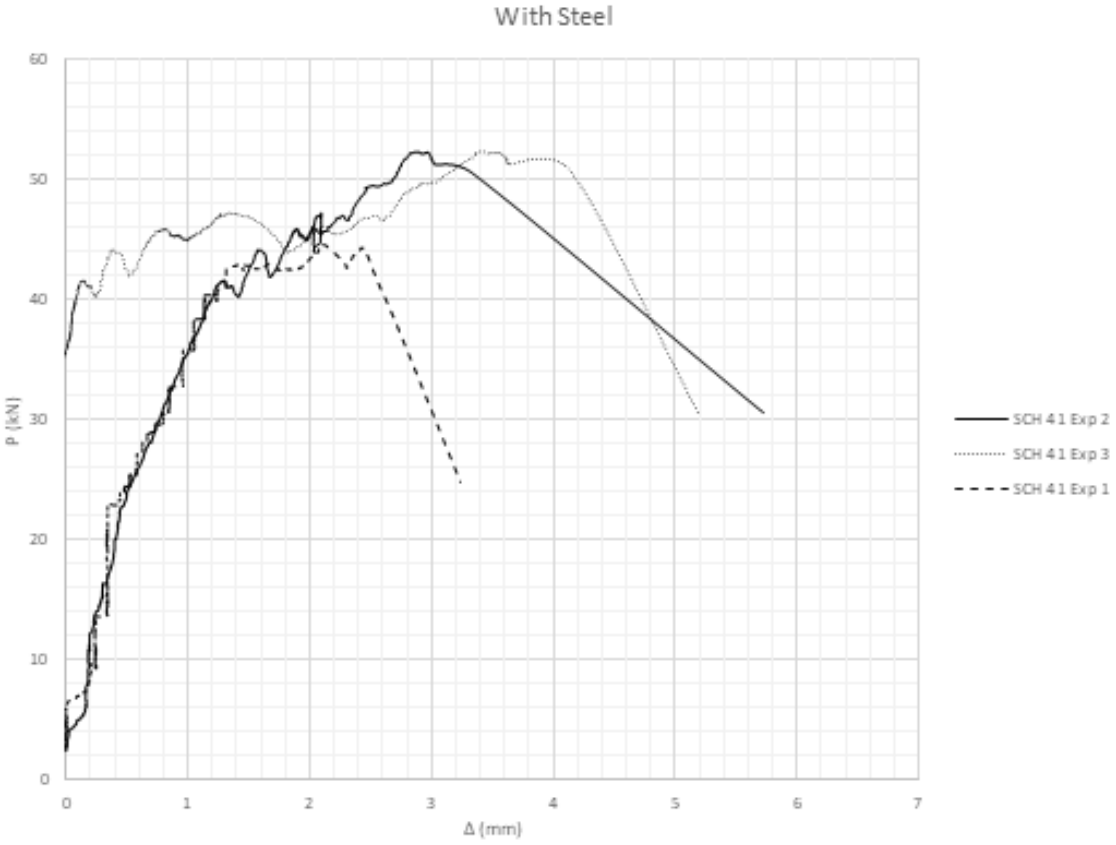
With Steel
P (kN)
Δ (mm)
SCH 41 Exp 2
SCH 41 Exp 3
SCH 41 Exp 1

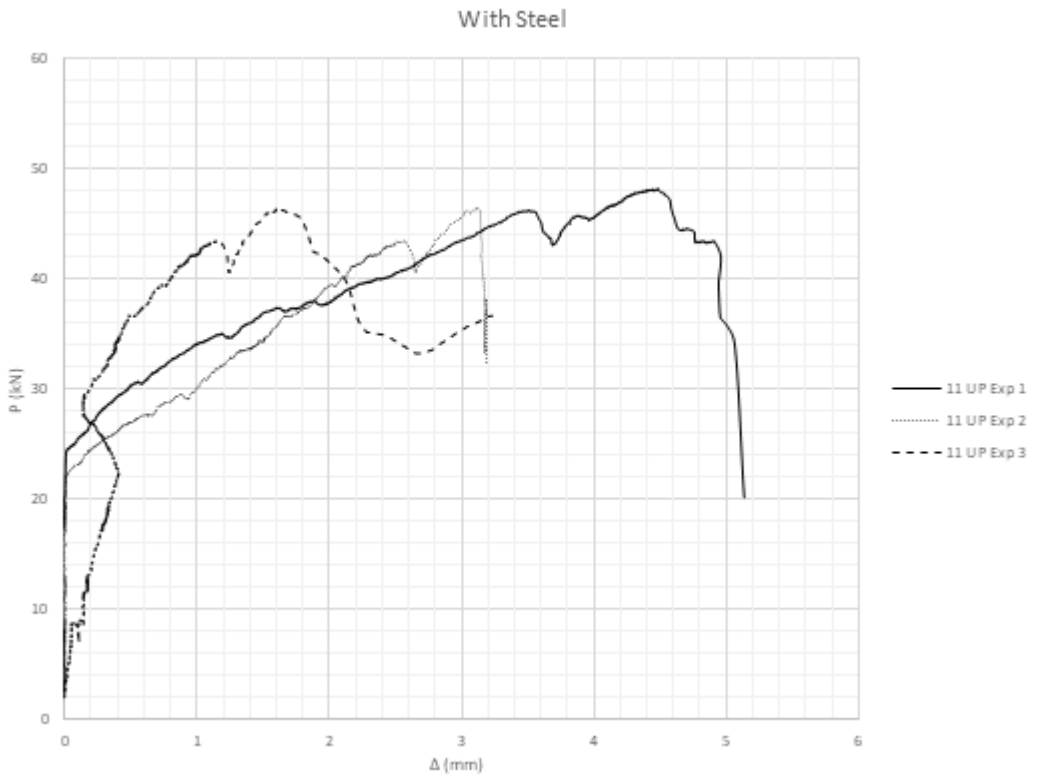
With Steel
P (kN)
Δ (mm)
11 UP Exp 1
11 UP Exp 2
11 UP Exp 3

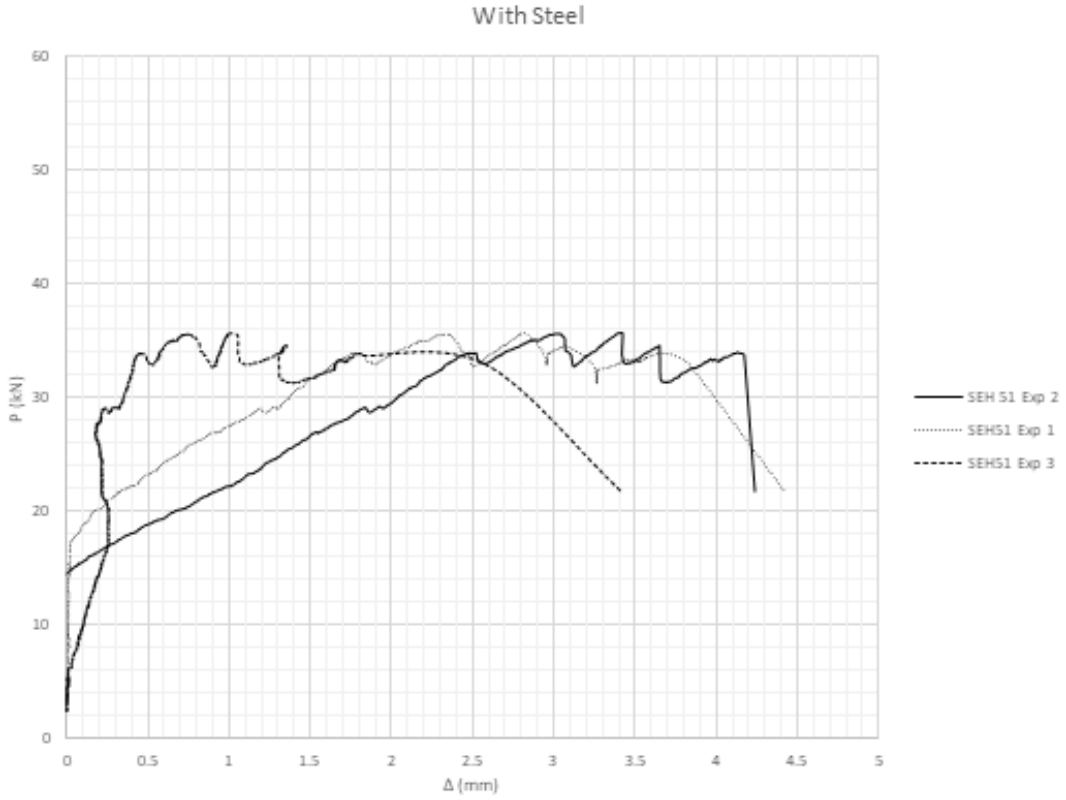
With Steel
P (kN)
Δ (mm)
SEH 51 Exp 2
SEH51 Exp 1
SEH51 Exp 3

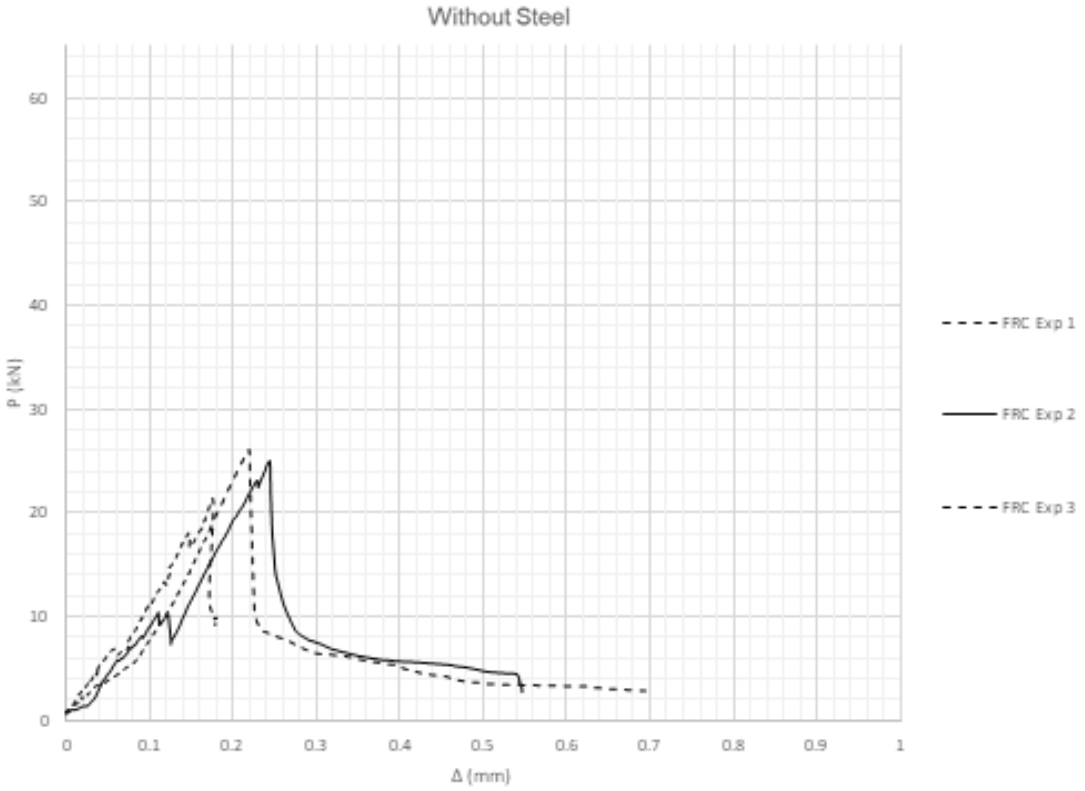
Without Steel
P (kN)
Δ (mm)
FRC Exp 1
FRC Exp 2
FRC Exp 3

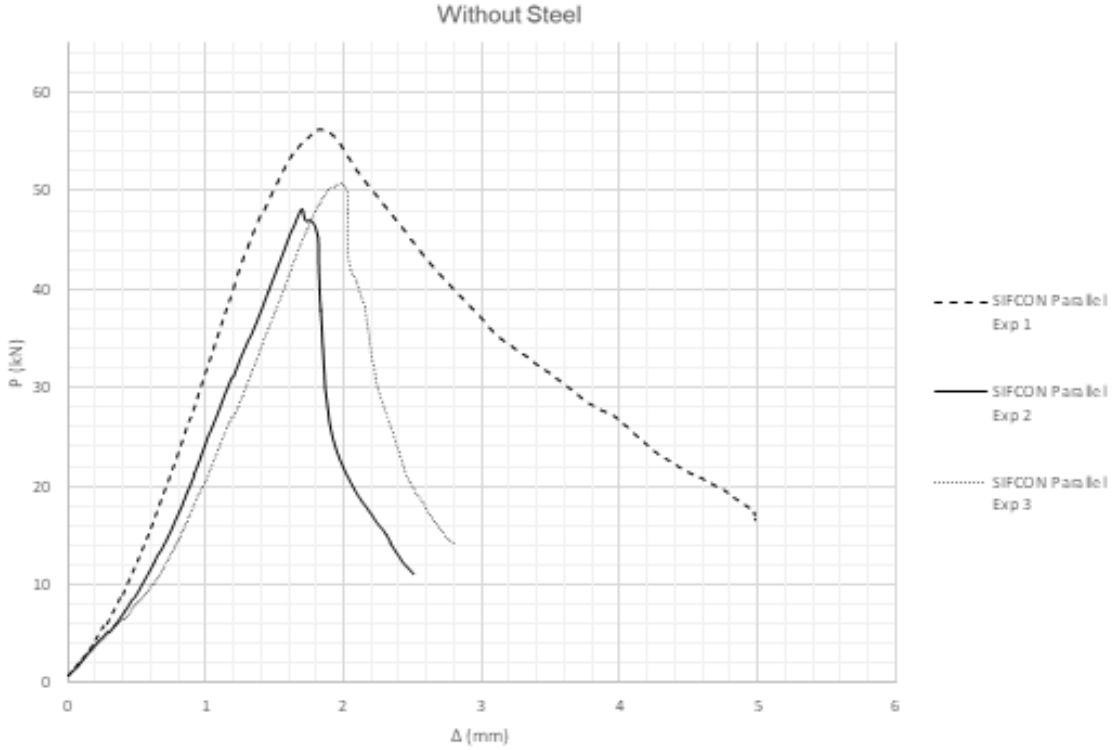
Without Steel
P (kN)
Δ (mm)
SIFCON Parallel Exp 1
SIFCON Parallel Exp 2
SIFCON Parallel Exp 3

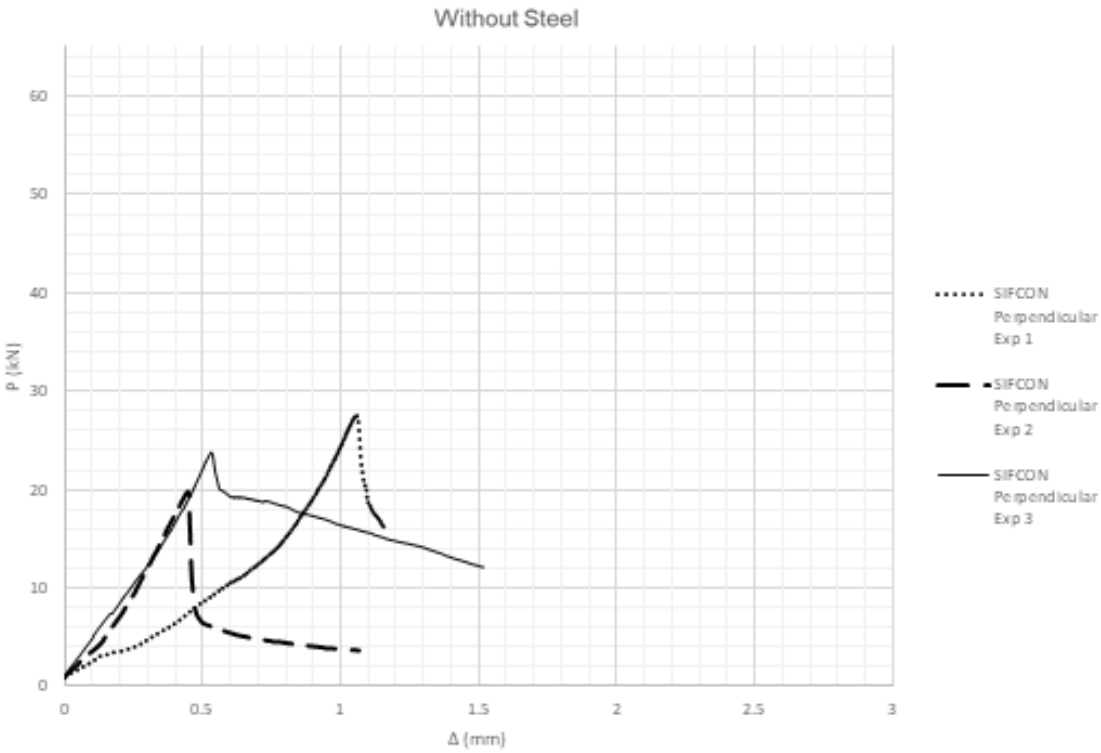
Without Steel
P (kN)
Δ (mm)
0
10
20
30
40
50
60
0
0.5
1
1.5
2
2.5
3
SIFCON Perpendicular Exp 1
SIFCON Perpendicular Exp 2
SIFCON Perpendicular Exp 3

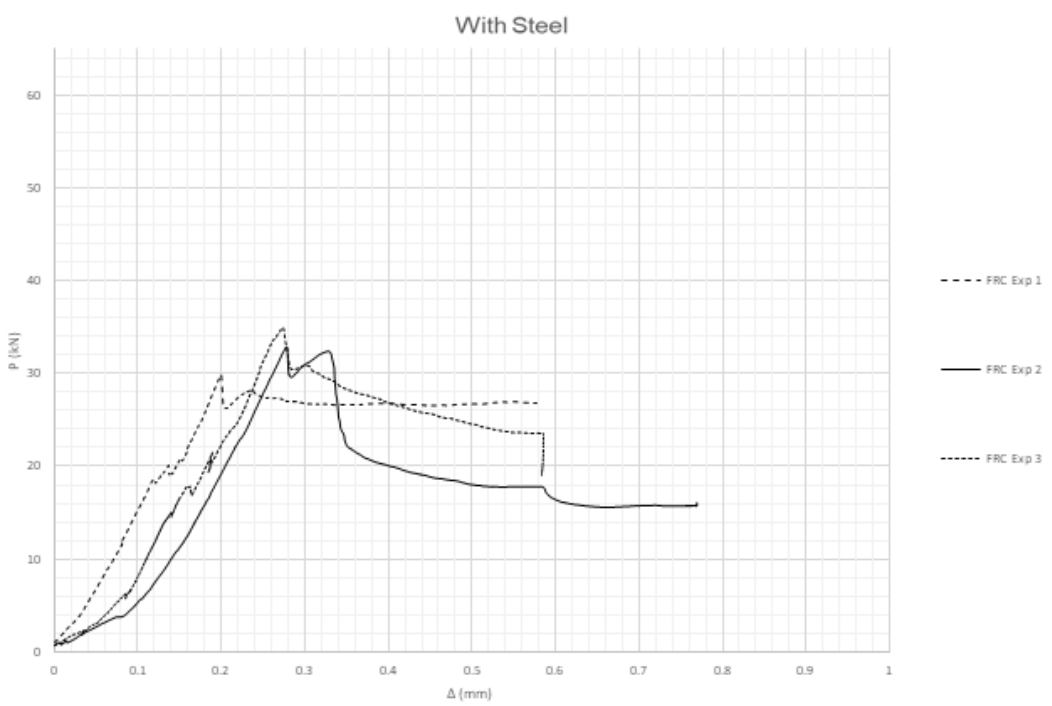
With Steel
P (kN)
Δ (mm)
0
10
20
30
40
50
60
0
0.1
0.2
0.3
0.4
0.5
0.6
0.7
0.8
0.9
1
FRC Exp 1
FRC Exp 2
FRC Exp 3

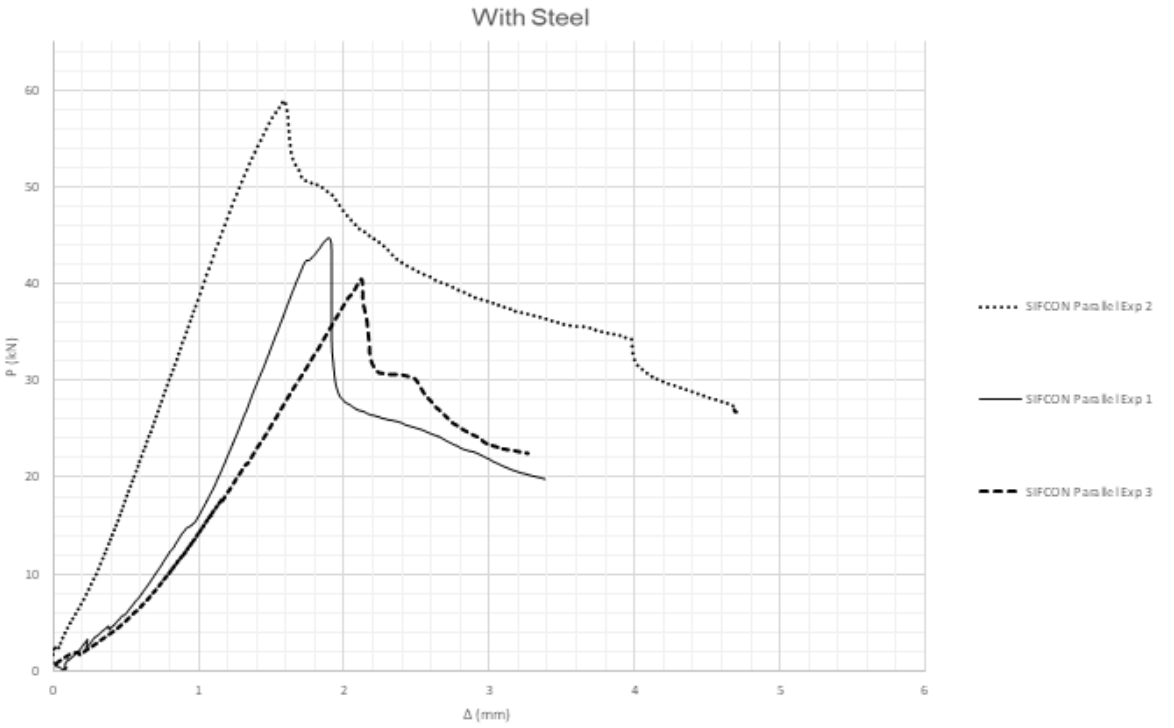
With Steel
P (kN)
Δ (mm)
SIFCON Parallel Exp 2
SIFCON Parallel Exp 1
SIFCON Parallel Exp 3

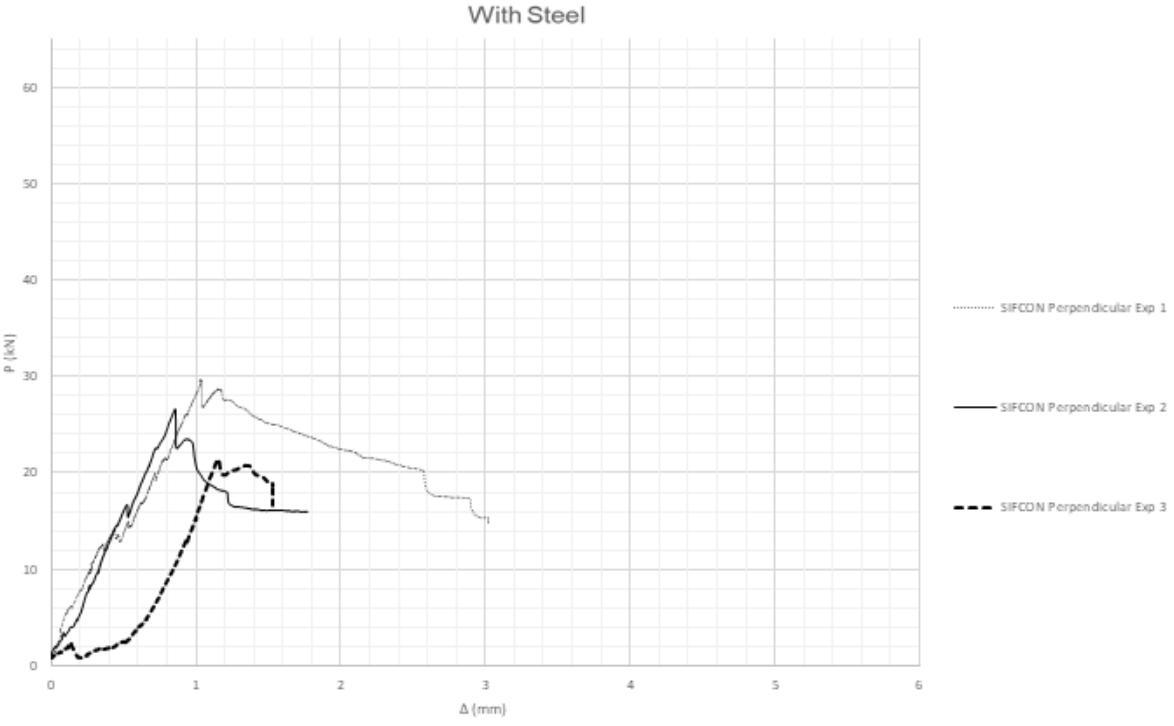
With Steel
P (kN)
Δ (mm)
SIFCON Perpendicular Exp 1
SIFCON Perpendicular Exp 2
SIFCON Perpendicular Exp 3

Without Steel

		Δcr	Pcr	Δy	Py	Δ_U	P_U	Δ_{R1}	P_{R1}	Δ_{R2}	P_{R2}	μ	Stiffness Ky	Ey	Stiffness Kc	Ec	T	TI
		mm	kN	mm	kN	mm	kN	mm	kN	mm	kN		kN/mm	kN/mm2	kN/mm	kN/mm2	kN-mm	
Regular Concrete	Test 1	0.09	5.78	0.31	8.14	0.40	8.97	-	-	0.45	0.00	1.45	10.93	16.47	61.49	92.67	2.54	1.00
	Test 2	0.10	5.83	0.29	8.19	0.42	9.04	-	-	0.42	0.00	1.45	12.50	1.88	57.73	8.70	2.70	1.00
	Test 3	0.11	5.86	0.27	8.10	0.38	9.01	-	-	0.40	0.00	1.48	14.00	21.10	53.27	80.28	2.38	1.00
GLASS SEH - 51	Test 1	0.17	7.16	0.55	18.61	2.39	43.54	-	-	2.43	0.00	4.43	30.27	31.71	41.89	6.31	44.56	16.48
	Test 2	0.12	9.07	0.59	21.30	2.82	32.65	-	-	3.56	0.00	6.03	26.08	39.30	74.34	112.04	67.88	25.10
	Test 3	0.05	7.72	0.28	21.95	2.26	32.51	-	-	2.27	0.00	8.11	61.88	93.26	154.40	232.69	57.63	21.31
CARBON 11- UP	Test 1	0.06	10.14	0.73	23.26	3.93	39.30	-	-	4.47	0.00	6.14	19.63	29.59	169.00	254.69	111.70	41.30
	Test 2	0.10	9.30	0.41	19.16	1.75	27.30	-	-	2.49	0.00	6.07	31.40	47.33	96.90	146.03	36.05	13.33
	Test 3	0.07	8.19	0.57	20.14	1.75	39.30	-	-	2.40	0.00	4.21	24.00	16.82	113.69	17.13	42.27	15.63
CARBON SCH - 41	Test 1	0.08	8.14	0.16	18.74	3.19	50.37	-	-	3.32	0.00	20.75	130.91	197.29	103.04	155.28	106.05	39.21
	Test 2	0.09	16.93	0.91	23.26	2.72	49.86	-	-	2.93	0.00	3.24	7.76	11.70	186.04	280.38	83.43	30.85
	Test 3	0.17	8.00	0.51	21.35	1.76	50.33	-	-	2.07	0.00	4.08	39.26	19.25	48.19	7.26	50.49	18.67
FRC	Test 1	0.05	6.36	0.08	9.31	0.17	20.91	-	-	0.19	9.09	2.35	101.69	153.25	124.63	187.82	3.11	1.15
	Test 2	0.05	5.73	0.07	9.72	0.24	24.30	-	-	0.55	3.37	8.27	199.35	300.43	124.63	187.82	3.92	1.45
	Test 3	0.05	4.97	0.06	8.45	0.22	25.54	-	-	0.69	2.80	11.19	348.00	27.47	95.58	14.40	3.70	1.37
SIFCON Parallel	Test 1	0.13	5.45	-	-	1.84	56.29	-	-	7.82	1.10	60.15	21.23	2.10	41.92	63.18	66.70	24.66
	Test 2	0.07	6.19	-	-	1.78	47.67	-	-	7.61	1.20	113.58	23.45	2.27	92.36	13.92	40.54	14.99
	Test 3	0.16	5.86	-	-	2.00	50.50	-	-	7.27	1.64	45.44	22.10	1.89	36.61	55.18	54.47	20.14
SIFCON Perpendicular	Test 1	0.12	4.52	-	-	1.06	27.48	-	-	1.80	4.70	15.00	26.50	3.76	37.69	56.80	15.35	5.68
	Test 2	0.07	5.90	-	-	0.46	19.51	-	-	2.70	3.57	40.30	43.20	3.84	88.10	13.28	5.21	1.93
	Test 3	0.09	5.90	-	-	0.54	23.62	-	-	2.10	5.30	23.60	31.15	3.68	66.33	99.96	6.86	2.54

With Steel

		Δcr	Pcr	Δy	Py	Δ_U	P_U	Δ_{R1}	P_{R1}	Δ_{R2}	P_{R2}	μ	Stiffness Ky	Ey	Stiffness Kc	Ec	T	TI
		mm	kN	mm	kN	mm	kN	mm	kN	mm	kN		kN/mm	kN/mm2	kN/mm	kN/mm2	kN-mm	
Regular Concrete	Test 1	0.09	1.33	0.34	5.19	0.51	7.53	-	-	0.82	5.11	2.40	15.55	23.43	14.34	21.62	5.13	1.00
	Test 2	0.09	1.28	0.35	5.24	0.49	7.42	-	-	0.78	4.97	2.23	15.29	23.04	14.07	21.20	3.59	1.00
	Test 3	0.09	1.35	0.33	5.18	0.50	7.63	-	-	0.84	5.32	2.55	15.89	23.95	15.17	22.86	4.14	1.00
GLASS SEH - 51	Test 1	0.07	8.56	0.36	21.95	2.84	35.54	4.43	21.77	15.31	0.00	12.43	46.19	47.15	129.67	19.54	121.55	23.70
	Test 2	0.02	15.07	0.93	21.86	3.05	35.50	4.24	21.77	15.19	0.00	4.54	7.45	11.22	717.62	1081.48	111.73	21.78
	Test 3	0.08	8.79	0.25	18.84	0.77	35.49	3.41	21.77	15.45	0.00	13.44	57.74	87.01	109.89	165.60	92.43	18.02
CARBON 11- UP	Test 1	0.05	8.79	0.47	29.86	4.50	47.95	5.14	20.19	15.13	0.00	10.95	50.40	75.96	172.37	259.77	186.82	36.42
	Test 2	0.13	8.79	0.64	27.58	3.14	46.00	3.19	32.14	15.08	0.00	5.00	37.06	55.85	67.62	101.91	103.74	20.23
	Test 3	0.15	8.61	0.41	22.05	1.66	46.19	3.24	36.65	15.10	0.00	7.86	50.34	34.72	59.34	8.94	112.72	21.98
CARBON SCH - 41	Test 1	0.24	9.26	0.45	23.30	2.10	44.37	3.23	24.79	15.11	0.00	7.25	68.18	102.76	38.57	58.12	99.61	19.42
	Test 2	0.14	7.21	0.44	22.93	2.92	52.19	5.73	30.61	15.30	0.00	12.98	52.75	25.62	50.42	7.60	214.27	41.78
	Test 3	0.10	6.88	0.37	37.35	3.41	52.37	5.19	30.61	15.12	0.00	14.01	113.68	171.31	67.49	101.71	216.30	42.17
FRC	Test 1	0.05	6.36	0.07	9.70	0.20	29.05	8.10	3.51	15.12	0.00	124.62	257.31	20.29	122.23	18.42	5.31	1.03
	Test 2	0.09	4.10	0.16	12.09	0.59	23.01	7.60	4.10	15.10	0.00	48.56	120.18	181.12	45.56	68.65	6.31	1.23
	Test 3	0.08	6.55	0.12	11.24	0.59	23.16	7.30	3.34	14.87	0.00	62.93	146.41	220.64	77.99	117.53	7.31	1.42
SIFCON Parallel	Test 1	0.07	4.57	-	-	1.91	44.00	7.20	8.10	14.70	0.00	102.86	33.21	3.23	65.26	98.35	182.65	35.61
	Test 2	0.06	7.61	-	-	1.60	58.42	8.05	7.02	15.10	0.00	129.84	36.20	3.55	122.81	18.51	262.04	51.09
	Test 3	0.05	5.10	-	-	2.13	39.68	6.95	6.10	15.31	0.00	131.13	34.71	3.46	96.23	145.02	156.98	30.61
SIFCON Perpendicular	Test 1	0.07	5.74	-	-	1.04	28.80	7.98	3.87	15.20	0.00	120.91	30.81	2.81	86.89	13.10	130.37	25.42
	Test 2	0.07	5.11	-	-	1.24	16.68	6.89	4.00	14.67	0.00	98.43	27.21	2.47	72.94	109.93	71.34	13.91
	Test 3	0.09	2.40	-	-	1.43	19.69	8.20	5.10	15.35	0.00	91.11	26.11	2.13	26.71	40.25	98.81	19.27

11. REFERENCES

ACI 440.1R-06. (2006) Guide for the Design and Construction of Structural Concrete Reinforced with FRP Bars. Farmington Hills, MI: *American Concrete Institute*.

ACI 440.2R-17. (2019) Guide for the Design and Construction of Structural Concrete Reinforced with Fiber-Reinforced Polymer (FRP) Bars. Farmington Hills, MI: *American Concrete Institute*.

ACI 318-11. Section 6-3 (2011). Building Code Requirements for Stuctural Concrete. Farmington Hills, MI: *American Concrete Institute*.

ANBAO Corp., Wire & Wire Products, 33 Qinhuangxi Street, Quihuangdao, P.R. China 066000, www.anbao.net, anbao@anbao.com, anbaowire@gmail.com

Azhari, M. F., Ismail, M. A., & Bakri, A. M. (2008). Use of SIFCON for retrofitting reinforced concrete beams with insufficient flexural capacity. Journal of Constructional Steel Research, 64(2), 157-166. https://doi.org/10.1016/j.jcsr.2007.06.002

Bakhshi, H., Shariati, M., & Raji, Y. (2019). Flexural behavior of reinforced concrete beams retrofitted with CFRP sheets. Journal of Composites for Construction, 23(5), 04019021. https://doi.org/10.1061/(ASCE)CC.1943-5614.0000945

Bencardino, F., Condello, A., & Ombres, L. (2016). Numerical and analytical modeling of concrete beams with steel, FRP, and hybrid FRP-steel reinforcements. *Composite Structures*, *140*, 53–65. https://doi.org/10.1016/j.compstruct.2015.12.045

El-Sayed, A., El-Salakawy, E., & Benmokrane, B. (2005). Shear strength of one-way concrete slabs reinforced with fiber-reinforced polymer composite bars. *Journal of Composites for Construction*, *9*(2), 147–157. https://doi.org/10.1061/(asce)1090-0268(2005)9:2(147)

fib Task Group 5.4. (2013). Model Code for Concrete Structures 2010: Final Draft, Volume 1. International Federation for Structural Concrete (fib). https://www.fib-international.org/publications/fib-model-code-2010.html

Fyfe Co. LLC, Fyfe Europe S.A. info@fyfe.com, www.fyfeco.com

Kim, D. (2018). Improvement for construction of concrete-wall with resistance to gas-

explosion. *Advances in Materials Science and Engineering*, *2018*, 1–9. https://doi.org/10.1155/2018/5189496

Krstulovic-Opara, N., Malak, S., "Tensile Behavior of Slurry Infiltrated Mat Concrete (SIMCON)", ACI Materials Journal, 1997, pp.39-46

Parametric study on design variables of concrete beam reinforced with GFRP rebar using finite element analysis. (2008). *Journal of the Korea Concrete Institute*, *20*(3), 357–367. https://doi.org/10.4334/jkci.2008.20.3.357

Naaman A.E., Homrich J.R. (1989). "Tensile Stress-Strain Properties of SIFCON" ACI Materials Journal, V. 86, No.3.

Naaman, A. E., Reinhardt, H. W., Fritz, C., & Alwan, J. (1993). Non-linear analysis of RC beams using a SIFCON matrix. Materials and Structures, 26(9), 522–531. https://doi.org/10.1007/bf02472863

Qureshi, S. A., & Saleem, M. U. (2018). Experimental investigation of flexural and shear strain characteristics of CFRP strengthened RC beams. Composite Structures, 193, 145-155. https://doi.org/10.1016/j.compstruct.2018.02.090

Rostásy, J. R., & Hegger, J. (2008). Shear Strength of Reinforced Concrete Beams with Fiber-Reinforced Polymer Reinforcement. ACI Structural Journal, 105(4), 387-394.

Sary A. Malak, & Neven Krstulovic-Opara. (2019). Micromechanical tensile behavior of slurry infiltrated mat concrete with inclined fibers. ACI Materials Journal. https://doi.org/10.14359/51714453

State of the Art Report on Fiber Reinforced Concrete. American Concrete Institute. Farmington, Michigan: ACI Committee 544, 2002.

Teng, J. G., Yuan, H., & Chen, J. F. (2006). FRP-to-concrete interfaces between two adjacent cracks: Theoretical model for debonding failure. *International Journal of Solids and Structures*, *43*(18-19), 5750–5778. https://doi.org/10.1016/j.ijsolstr.2005.07.023

Tyfo® SCH-11UP Composite using Tyfo® S-Epoxy. Singapore: FYFE Asia Pte Ltd.

Tyfo® SEH-51A Composite using Tyfo® S-Epoxy. Singapore: FYFE Asia Pte Ltd.

T.Y. Lim, P. Paramasivam, and S. L. Lee Analytical model for tensile behavior of steel-fiber concrete. (1987). *ACI Materials Journal*, *84*(4), 284-290. https://doi.org/10.14359/1454

Wang, Y. C., & Chen, C. H. (2003). Analytical study on reinforced concrete beams strengthened for flexure and shear with composite plates. Composite Structures, 59(1), 137–148. https://doi.org/10.1016/s0263-8223(02)00171-x

Yang, J. M., Yoo, D. Y., Shin, H. O., & Yoon, Y. S. (2011). Flexural Strength and Deflection Evaluation for FRP Bar Reinforced HSC Beams with Different Types of Reinforcing Bar and Fiber. *Journal of the Korea Concrete Institute*, *23*(4), 413–420.

Zhao, T., Wu, C., Li, Y., & Zou, D. (2014). Finite element modeling of reinforced concrete beams retrofitted with SIFCON under flexural loading. Journal of Materials in Civil Engineering, 26(7), 1402-1411. https://doi.org/10.1061/(ASCE)MT.1943-5533.0000892